# Entanglement Transition of Randomly Branched Polymers in the Hyperbranched Class

**Suneel Kunamaneni,[†] D. Martin A. Buzza,*[,‡] Daniel J. Read,[§] David Parker,[||] Alan M. Kenwright,[||] W. James Feast,[||] and Anne L. Larsen[⊥]**

*IRC in Polymer Science and Technology, School of Physics and Astronomy, University of Leeds, Leeds LS2 9JT, U.K., Department of Physics, University of Hull, Hull HU6 7RX, U.K., School of Mathematics, University of Leeds, Leeds LS2 9JT, U.K., IRC in Polymer Science and Technology, Department of Chemistry, University of Durham, Durham DH1 3LE, U.K., The Danish Polymer Centre, Technical University of Denmark, DK-2800 Kgs, Lyngby, Denmark*

*Received February 13, 2006; Revised Manuscript Received June 23, 2006*

ABSTRACT: We study the melt rheology of randomly branched polymers in the hyperbranched polymer (HBP) class which are formed by the co-condensation of AB and $AB_2$ type monomers. Specifically, we study the effect of branch length $M_x$ on the entanglement transition in the HBP class. To this end, two series of HBPs were prepared using $AB_2$ mole fractions of 10% and 1% respectively. This allowed us to vary $M_x$ from just below to just above $M_e$, the entanglement molecular weight for linear chains of the same chemistry. For the 10% branched samples ($M_x < M_e$), we were able to quantitatively model the low and intermediate frequency rheology data using a Rouse model for unentangled chains. For the 1% branched samples ($M_x > M_e$), there is a clear entanglement plateau for the higher molecular weight samples and we were able to quantitatively model the rheology around the entanglement plateau region using the tube model. Our data demonstrate conclusively that the entanglement transition for randomly branched polymers in the HBP class is controlled by $M_x$ and the transition occurs around $M_x \approx M_e$. These conclusions are the same as for randomly branched polymers in the percolation class. We are able to explain these results using either the Colby−Rubinstein model or double reptation model for entanglements if we assume that whole molecules *and* side branches with Rouse times less than the Rouse time of an entanglement do not contribute to entanglement formation.

## 1. Introduction

The entanglement transition is one of the most fundamental dynamic transitions in polymer systems. For monodisperse linear polymer melts, it is well established that the entanglement transition is controlled by the chain length or molecular weight $M$ and the transition occurs at $M = M_c \approx 2M_e$, where $M_e$ is the entanglement molecular weight, a material specific parameter. The entanglement transition is accompanied by a sharp change in slope in the viscosity $\eta_0$ vs $M$ curves such that[1−3]

$$\eta_0 = KM, \quad M < M_c$$

$$\eta_0 = KM^{3.4}, \quad M > M_c$$

where $K$ is a temperature-dependent constant.

However many commercially important polymers are not linear but randomly branched, for example low-density polyethylene (LDPE) and metallocene-catalyzed polyolefins. For randomly branched systems, the entanglement transition is considerably more complex for several reasons. First, there are many mass scales in these systems, and it is not clear which of these control the entanglement transition. Possible candidates include the branch length $M_x$ (i.e., the molecular weight of chain portions between branch points), the span length (i.e., the molecular weight of the longest linear path through the branched molecule) and the total molecular weight, all appropriately averaged over the ensemble. Second, it is not clear where the entanglement transition occurs in relation to these mass scales.

For randomly branched polymers in the percolation class (e.g., polymer gels, vulcanized rubbers), the entanglement transition has been studied in detail in the seminal work of Colby and co-workers.[4−6] These authors studied the dynamic critical exponents of various percolation systems close to the gel point as a function of the branch length $M_x$. In particular in ref 6, they collate data from their own studies and the literature and find that dynamic critical exponents assumed unentangled Rouse values for $M_x < 2M_e$, and non-Rouse values for $M_x > 2M_e$ due to the effect of entanglements. Their study therefore shows conclusively that the entanglement transition for randomly branched polymers in the percolation class is controlled by the branch length $M_x$ and the transition occurs around $M_x \approx M_e$.

This is a nontrivial result. In this paper, we wish to study whether the same result also holds true for other randomly branched polymer systems. Specifically we choose to study randomly branched polymers in the hyperbranched polymer (HBP) class. The best known system in this class is randomly branched polymers formed from a one-pot polycondensation of $AB_2$ monomers, where the chemistry is such that A reacts exclusively with B.[7,8] This route produces short chain branched HBPs which have potential applications as rheology modifiers for polymer processing.[9,10] Recently Read and McLeish[11] have shown that under certain reactor conditions (i.e., steady state continuous stirred tank reactor, CSTR), metallocene-catalyzed randomly branched polyolefins also belongs to the HBP class. This route produces long chain branched HBPs with controlled long chain branching and opens up the possibility of producing

* To whom correspondence should be addressed. E-mail: d.m.buzza@hull.ac.uk.

[†] IRC in Polymer Science and Technology, School of Physics and Astronomy, University of Leeds.

[‡] Department of Physics, University of Hull.

[§] School of Mathematics, University of Leeds.

[||] IRC in Polymer Science and Technology, Department of Chemistry, University of Durham.

[⊥] The Danish Polymer Centre, Technical University of Denmark.

10.1021/ma0603276 CCC: $33.50 
Published on Web 08/17/2006

branched polyolefins with tailored properties on a commercial scale.[12]

Motivated by the study of Colby and co-workers, we study the effect of branch length variation on the entanglement transition of HBPs. The HBPs used in this study are produced by the one pot condensation route and in order to vary the branch length, we mixed in different proportions of AB monomers in the polycondensation reaction. To bracket the transition fairly tightly, we prepared two series of HBPs, one where $M_x$ was just below $M_e$ and another where $M_x$ was just above $M_e$. Unfortunately, unlike percolation systems, there is no gel point for HBP systems because the gel point is destroyed by nonmean field fluctuations.[13,14] (In the context of randomly branched polymers, fluctuations refer to fluctuations in the number of characteristic polymers within a characteristic volume.[15,16] When these fluctuations become large (relative to the mean value), intramolecular loops and excluded volume interactions also become important. Following ref 16, we therefore use the shorthand "fluctuations" to refer to all of these phenomenon.) Because of the absence of a gel point, it is not possible to characterize the degree of entanglement of a HBP system by measuring dynamic critical exponents. Instead we characterize the degree of entanglement by quantitatively analyzing the dynamic moduli (i.e., $G'$, $G''$) of HBPs over a wide frequency range. In the unentangled regime, we fit the rheology data using the Rouse model.[17] In the entangled regime, we fit the rheology data using a tube model adapted for long chain branched HBPs which is described in detail in appendix A.

We note that previous authors have also sought to model the rheology of entangled randomly branched polymers using the tube model. For example Kasehagen et al.[18] have fitted $G'$, $G''$ for long chain branched polybutadiene using the McLeish and O'Conner model for star-linear blends.[19] McHugh and co-workers[20] have also fitted $G'$ and $G''$ for HBPs similar to ours using a tube model for Cayley trees (i.e., long chain branched dendrimers) developed by Blackwell et al..[21] However in both studies, the spacer "seniority distribution" that was used is strictly speaking not correct (see section 3.3.2 for a definition of seniority). In our study, we first determine the branch length and branching probability for all our samples via NMR measurements coupled to a detailed reaction kinetics model. Using the branching probability, we then calculate the spacer seniority distribution for all our HBP samples from first principles using the recent theory of Read and McLeish.[11]

The rest of the paper is organized as follows. In section 2, we describe the experimental details of our study, including the synthesis of the HBPs, SEC, DSC, NMR and rheology. In section 3, we describe the theory used to model the experimental data, including the static scaling model used to analyze the SEC data, the reaction kinetics model used to analyze the NMR data (in order to extract the branch length and branching probability), and the Rouse and tube model used to analyze the rheology data. In section 4, we discuss the results from our theoretical analysis of the experimental data. In particular, we find that the entanglement transition for HBPs is controlled by the branch length $M_x$ and the transition occurs around $M_x \approx M_e$. In section 5, we present scaling results to explain the entanglement transition for randomly branched polymers. Finally, in section 6, we present a summary of our conclusions.

## 2. Experimental Details

**2.1. Synthesis.** The hyperbranched polymers used in this study are aromatic polyesters synthesized from the AB and $AB_2$ monomers shown in Figure 1. Details of the monomer synthesis can be found in work by Keeney[22] and Anderson.[23] To study the effect of branch length variation on the entanglement transition, we synthesized samples with both 10 mol % and 1 mol % of branched monomers. For HBPs with mole% of branched monomers $\lesssim$20%, sample crystallization becomes an issue for this chemistry.[23] To suppress crystallization, a nominally 50:50 ratio of meta (M) and para (P) analogues was used for the AB monomers (the $AB_2$ monomers are referred to as T monomers). The amorphous nature of the resultant HBPs meant that we could perform melt rheology at significantly lower temperatures where sample drying conditions are no longer critical.

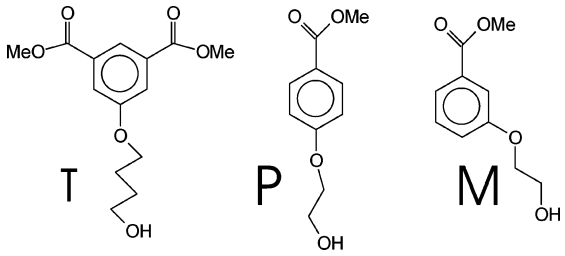


**Figure 1.** Monomers used for the synthesis of HBPs.

The synthesis of the HBPs proceeded as follows. The monomers were dried and added to the reaction vessel. Titanium tetrabutoxide, a thick viscous liquid, was then added as a transesterification catalyst in the ratio 1 mg:1 g (catalyst:monomer) using a microliter syringe. Titanium tetrabutoxide reacts with residual traces of water to form hydroxy titanate species with no catalytic activity. Consequently, in an attempt to exclude moisture from the reactor, glassware was routinely flamed and cooled under dry nitrogen before use. Upon reassembly, the reactor was heated to 150 °C using an oil bath. Molten monomers were then mixed by a two paddle stirrer, designed to ensure good mixing in both the vertical and horizontal directions. The temperature of the polymerization vessel was increased to 240 °C at a rate of 10 °C $min^{-1}$ and maintained throughout the reaction. Methanol, an unwanted side-product, was removed by sweeping the polymerization vessel with a slow stream of dry nitrogen. This helped to drive the equilibrium to high conversion and minimize the effects of oxidative degradation. To synthesize both 10 mol % and 1 mol % samples of varying molecular weights, the polymerization was quenched at different reaction extents.

**2.2. SEC and DSC.** SEC characterization was performed on a PL-GPC 220 system (Polymer Labs.) at 40 °C in THF + 10% acetic acid (acetic acid was added to suppress the ionic exclusion effect[24]). The column set consisted of two 7.5 mm diameter × 300 mm long, 5 $\mu$m particle diameter mixed-C Polystyrene-Divinyl Benzene gel columns (pore sizes of $10^2$, $10^3$, and $10^5$Å). The injection volume was 200 $\mu$L and flow rate was 1.0 mL/min with sample concentrations around 2 mg/mL. A differential refractive index (DRI) detector, a viscometer (Viscotek model 220R) and a PD2040 two angle laser light scattering (TALLS) detector (Precision detectors Inc.) were used in conjunction with SEC. The specific refractive index increment $dn/dc$ in THF + 10% acetic acid was about 0.17 ± 0.003 mL/g at 670 nm for the HBP samples. The analysis technique assumed a random coil model and the molar mass for each elution volume was calculated using the 15° LS signal. The weight-average molecular weights $M_w$ were calculated by integrating the 15° LS signal alone (corrected using the form factor for the random coil model) as this represents the most accurate and precise measure of $M_w$ by SEC with light scattering detection.[25,26]

Thermal properties were measured using DSC on a Perkin-Elmer Pyris 7. The polymer samples were annealed at 250 °C and cooled at a rate of 50 °C $min^{-1}$ to 30 °C. DSC measurements were made over a temperature range of 30−250 °C using a heating rate of 10 °C $min^{-1}$. The value for the glass transition temperature $T_g$ was taken as the temperature at the midpoint of the observed $\Delta C_p$. All the samples showed a single glass transition with no evidence of melting or crystallization peaks, confirming that the samples are amorphous.

The $M_w$ and $T_g$ values for the 10 mol % and 1 mol % HBPs are collected in Table 1. The HBP samples are identified by the mole

**Table 1. Properties of Polymers Studied in This Paper**

| sample | $M_w$ (g/mol) | $T_g$ (°C) |
|---|---|---|
| H10-20 | 20 300 | 51.5 |
| H10-32 | 31 900 | 52.4 |
| H10-65 | 64 500 | 55.0 |
| H10-120 | 119 900 | 54.0 |
| H10-256 | 256 100 | 55.0 |
| H1-18 | 18 300 | 56.2 |
| H1-43 | 42 600 | 57.4 |
| H1-63 | 62 900 | 59.9 |
| H1-76 | 75 600 | 59.6 |

**Table 2. Monomer Composition from Ar−O Region of Spectrum for H1 and H10 Series**

| sample | mol % P | mol % M | mol % T |
|---|---|---|---|
| H10-20 | 37.5 | 49.5 | 13.0 |
| H10-32 | 41.0 | 46.8 | 12.3 |
| H10-65 | 38.8 | 48.0 | 13.2 |
| H10-120 | 41.4 | 44.3 | 14.3 |
| H10-256 | 37.9 | 45.2 | 17.0 |
| H1-18 | 49.8 | 49.1 | 1.1 |
| H1-42 | 49.4 | 49.5 | 1.1 |
| H1-63 | 49.2 | 49.3 | 1.5 |
| H1-76 | 49.7 | 48.8 | 1.5 |

percent content of $AB_2$ monomers and their weight-average molecular weight. Thus, H10-120 refers to a HBP sample containing 10 mol % of $AB_2$ monomer with a weight-average molecular weight of $120 \times 10^3$g/mol.

**2.3. NMR.** NMR spectra were recorded in 5 mm o.d. tubes containing samples dissolved in $CDCl_3$. Measurements were made at ambient probe temperature using a Varian Inova-500. Quantitative $^{13}C$ spectra were recorded at 125.67 MHz using a 45° pulse, 1.4 s acquisition, and 8.6 s recycle delay with inverse-gated proton decoupling. Quantitation was checked by repeating the measurement for one sample with the recycle delay increased to 30 s.

As a starting point for assignment of the peaks, we looked at the spectra obtained from samples prepared by homopolymerization of T monomers[27] and by copolymerization of a nominally 50:50 mixture of P and M (see section 2.5). Using this information, and assuming approximately random polymerization, it was possible to assign all of the peaks in the spectra of the terpolymers to specific carbons in the monomer units. In particular, the region of the spectra corresponding to oxygen-bonded carbons in an aryl ring (157−164 ppm) contained signals which could easily be assigned to each of the three monomers. This allowed us to measure the mole% of each of the three monomers in the terpolymer samples. The monomer compositions for both H10 and H1 determined in this way are reported in Table 2. However in most regions, detailed analysis of the polymer microstructure was limited by spectral overlap.

It was found that the region of the spectra corresponding to the methylene signal from the $-CH_2-O-Ar$ moieties gave the best distribution of signals for all the possible species present, so detailed analysis concentrated on this area. Partial spectral overlap and the fact that line shapes were affected by chemical shift distributions meant that deconvolution assuming Lorentzian line shapes did not give reliable results, so analysis was based on simple integration of the peaks involved. As an example of the results obtained, the relevant region of the spectrum of H10-65 is shown in Figure 2 with the peaks assigned in terms of the monomer unit containing the relevant methylene group (first letter) and the monomer unit to which that methylene group is attached via an ester linkage (second letter). The observed intensities of the lines in this region (as a percentage of the total intensity of all the peaks) for different samples in the H10 series are reported in Table 3. Analogous information for the H1 series was unfortunately not available because the NMR signals pertaining to the T monomers were too low.

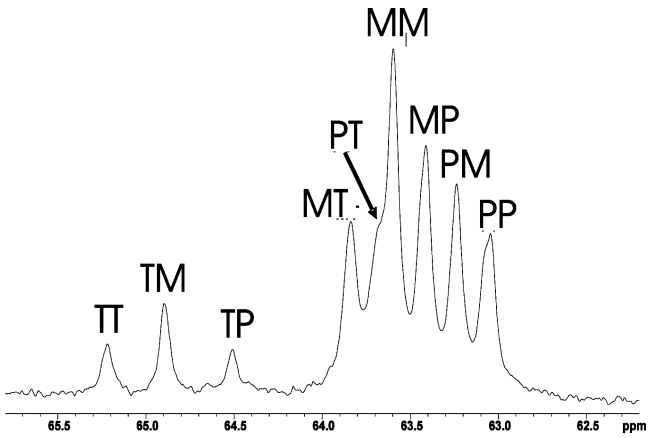


**Figure 2.** Peak assignment in the alkoxy region for sample H10-65.

**Table 3. Observed Peak Intensities (as a Percentage of Total Intensity for All the Peaks) in the Alkoxy Region**

| sample | TT | TM | TP | MT | PT + MM | MP | PM | PP |
|---|---|---|---|---|---|---|---|---|
| H10-20 | 3.1 | 5.0 | 2.7 | 11.0 | 29.2 | 17.8 | 16.5 | 14.8 |
| H10-32 | 3.5 | 5.4 | 3.7 | 12.4 | 28.1 | 17.4 | 15.9 | 13.7 |
| H10-65 | 3.5 | 5.7 | 3.3 | 13.1 | 30.9 | 16.5 | 15.7 | 11.4 |
| H10-120 | 3.2 | 5.8 | 3.8 | 11.9 | 27.8 | 16.1 | 16.6 | 14.7 |
| H10-260 | 6.4 | 7.2 | 5.0 | 14.6 | 27.8 | 14.1 | 13.0 | 11.9 |

**2.4. Rheology.** Small amplitude oscillatory shear experiments were carried out in the linear viscoelastic regime on a Rheometrics ARES controlled strain rheometer. For all our measurements we used a 10 mm diameter stainless steel parallel plate geometry. Frequency sweeps from 0.1 to 100 rad/s were performed at different temperatures above the glass transition temperature under a dry nitrogen atmosphere. Strain amplitudes varied from about 20% for the highest temperatures down to 0.02% for the lowest temperatures close to the glass transition temperature. To expand the range of achievable frequencies, time−temperature superposition (TTS) was employed to collapse the data at different temperatures onto master curves. Specifically the horizontal shift factor $a_T$ and the vertical shift factor $b_T$ were found by performing a 2D TTS of the data at different temperatures and $b_T$ was found to be of order unity in all cases ($0.9 \rightarrow 1.1$). To accommodate variations in sample compliance with temperature, measurements were performed at different gap settings ($0.5 \rightarrow 2.0$ mm). We used higher gaps close to $T_g$ since higher gaps reduce compliance issues. We observed that instrumental compliance is a problem only at the highest frequencies (close to the high-frequency crossover in the glassy regime). For lower frequencies in the glassy regime, different gap settings gave the same values of modulus. Since the primary focus of the paper is in the low and intermediate frequency rheology, the compliance problems encountered in the high-frequency glassy regime were not of serious concern.

**2.5. Entanglement Spacing from Linear Samples.** To obtain an independent measure of the entanglement weight $M_e$ for the chemistry used in this study, we also synthesized a linear polymer consisting of a nominally 50:50 ratio of M and P AB monomers using the same procedure outlined in section 2.1. SEC confirmed that the MWD of the linear polymer followed the most probable distribution with $M_w = 16\,900$ g/mol and $M_w/M_n \approx 2$. The entanglement length for this chemistry turns out to be rather short so that we were able to obtain a reasonable estimate of the entanglement length from our linear sample. The dynamic moduli of the linear sample was then measured and fitted to a theory that includes the single chain relaxation function $\mu(t)$ of Likhtman and McLeish,[28] the double reptation rule[29] with 2.2 power to account for constraint release of the matrix (i.e., tube), and fast and longitudinal Rouse modes as given in eq 19 of ref 28 (we are very grateful to Alexei Likhtman for performing the fitting for us). This procedure produced an entanglement molecular weight of $M_e =$ 2400 g/mol (in this paper, we use the "G" definition for the

entanglement weight,[30] see Appendix A). Using a monomer weight of $m_0 = 164$ g/mol, this corresponds to an entanglement degree of polymerization of $N_e \approx 15$ which is in excellent agreement with the value $N_e = 15.5$ obtained later from fitting the H1 rheology data using the tube model (see section 4.5).

## 3. Theory

**3.1. Molecular Weight Distribution.** When modeling the rheology of the H10 samples, we require as an input the molecular weight distribution (MWD) of the samples. To parametrize the MWD for H10, we assume that the number density distribution $n(M)$ (defined as the number of molecules with molecular weight $M$ *per monomer*) obeys the scaling form[14,17,25]

$$n(M) \sim M^{-\tau}\exp(-M/M_{\text{char}}) \quad (1)$$

where $\tau$ is the polydispersity exponent. Equation 1 defines the largest characteristic molecular weight $M_{\text{char}}$ for a given sample. In a previous study on HBPs with similar chemistry but shorter spacer lengths,[25] we found that $\tau$ was close to the mean field value of $\tau = 1.5$. Since we expect nonmean field fluctuations to decrease with increasing spacer length,[14] we assume $\tau = 1.5$ for both the H10 and H1 series. For $\tau < 2$, $M_{\text{char}}$ is proportional to $M_w$ in the limit $M_{\text{char}} \gg M_x$.[17] However as we shall see in section 4.1, this proportionality is not strictly obeyed for the H10 series, probably because not all the samples in the series have a high enough molecular weight to reach the asymptotic limit.

**3.2. Reaction Kinetics Model for Polycondensation Reaction.** As mentioned in the previous section, nonmean field fluctuations (e.g., intramolecular correlations between A and B groups, loop formation etc.) decrease with increasing branch length. We therefore expect mean field theory to be reasonable for the H10 series and very good for the H1 series. This fact allows us to use a mean field reaction kinetics model to predict the statistical properties of the HBP molecules arising from the polycondensation reaction.

In particular, for each of the samples in the H10 series, NMR results are available indicating the mole fraction of monomers P, M, and T and the relative concentration of reacted bonds of type $A_IB_J$ with I, J = P, M, or T, where P, M, and T refer to para AB monomers, meta AB monomers, and $AB_2$ monomers respectively (see Tables 2 and 3; note that $A_IB_J$ is equivalent to IJ in the notation of Table 3 and Figure 2). A simple reaction kinetics model is able to make predictions for these bond concentrations. We illustrate this by considering the particular case where all A groups are assumed to behave identically, but the B groups on different monomers react at different rates. We further assume that the two B groups on a T monomer react independently so that the reaction rate of each B group is unaffected by the reaction of the other B group. This assumption is justified by NMR measurements of the degree of branching (DB) of HBP samples formed purely by $AB_2$ monomers similar to the T monomers.[31,32] A value of DB = 0.5 is found, which implies that the reaction rates of the two B groups on the T monomer are independent.[33]

For the above assumptions, the state of the reaction ensemble is determined by the following parameters: the number fractions $f_M$, $f_P$, and $f_T$ of monomers present in the initial mixture; two ratios of reaction rate constants for the different B groups ($k_M/k_P$ and $k_T/k_P$), which to a first approximation should be held constant for a given chemistry, and one independent reaction probability (for example, the probability that a B unit on a P monomer has reacted). Since $f_M$, $f_P$, and $f_T$ can be measured for each sample, and we can fix the reaction probability variable from the sample average molecular weight, one can use the relative concentrations of reacted bonds of type $A_IB_J$ for the different samples to deduce the reaction rate constants. Details of this calculation are given in section 4.2. Alternative assumptions for the reactivity of the functional groups are also considered in section 4.2 (further details for both cases can be found in the Supporting Information).

Read and McLeish[11] have recently demonstrated that under mean field conditions, branched polymers in the HBP class can be directly mapped onto the distribution of branched molecules in metallocene-catalyzed polyolefins under certain reactor conditions (i.e., steady-state continuous stirred tank reactor, CSTR). Consequently, similar to the metallocene class, the topology of branched polymers in the mean field HBP class can be characterized by just two independent parameters:[7,11] an "upstream" branching probability, $b_U$ (the probability that a polymer strand chosen at random has a branchpoint in the "upstream" direction) and the (number) average branch degree of polymerization, $P_x$. In the context of mean field HBPs (i.e., no intramolecular loops so that each molecule has one and only one unreacted A group), the upstream and downstream directions correspond respectively to moving away from and toward the unreacted A along the molecule. Details of how $b_U$ and $P_x$ for H10 and H1 are calculated from the rate constants are given in section 4.3 (also see Supporting Information for further details).

**3.3. Rheology.** As we shall confirm later, the entanglement transition in HBPs is controlled by the branch length $N_x$ and the transition occurs around $N_x \approx N_e$, where $N_e$ is the entanglement length. (Note that in this paper, we use the symbols $N$ and $P$ to denote degree of polymerization and $M$ to denote molecular weight.) For the moment, we shall take this result as given and delay the discussion of this rather subtle point to section 5.

In practice of course, the branch lengths in our samples are not monodisperse but exponentially distributed according to the most probable distribution. Specifically the average branch length calculated from the reaction kinetics model $P_x$ is the number-average branch length of the ensemble. To make our rheological models tractable, we make a monodisperse branch length approximation and assume that the effective branch length $N_x$ is the weight-average branch length, i.e., $N_x = 2P_x$. For unentangled HBPs, this approximation is adequate within the dynamic scaling model. For entangled HBPs, this approximation is much more delicate. In the case of star polymers, the mutual retraction of star arms turns out to strongly self-average out the effect of polydispersity so that the rheology is primarily controlled by $M_w$ of the star arms.[34] On the other hand, for H-polymers, the presence of slowly relaxing cross-bar material amplifies the inherent polydispersity of the arm relaxation times so that the rheology of H-polymers becomes extremely sensitive to any polydispersity in the arm material.[35] On the basis of the latter, we might expect branch length polydispersity to play an important role in our system because of the presence of high seniority spacers. We point out that a recent algorithm developed by Das et al.[36] can explicitly account for branch length polydispersity in an HBP ensemble without the need for any preaveraging. However this level of modeling lies beyond the scope of the current study.

**3.3.1. Unentangled Regime.** For the H10 series we have $N_x < N_e$. We therefore assume that the HBP chains are unentangled and model the rheology using the dynamic scaling model of Rubinstein et al.[37] For an HBP ensemble with MWD given by

eq 1, we showed previously that the complex shear modulus is given by[17]

$$G^*(\omega) = \frac{d_R}{2}\frac{G_x}{\Gamma(2-\tau, a)}\int_0^{\epsilon_x}\left(\frac{\epsilon}{\epsilon_x}\right)^{(d_R/2)-1}\Gamma\left[2-\tau, a\left(\frac{\epsilon}{\epsilon_x}\right)^{-d_R/2}\right]\frac{i\omega}{i\omega+\epsilon}\frac{d\epsilon}{\epsilon_x} \quad (2)$$

where $d_R$ is the dimension of the relaxation rate spectrum, $G_x$ is the unrelaxed shear modulus of the HBP melt, $a = N_x/N_{char}$ ($N_{char}$ is the largest characteristic degree of polymerization of the ensemble), $\epsilon_x$ is the high relaxation rate cutoff associated with spacer relaxation and $\Gamma(b, z) = \int_z^\infty t^{b-1}e^{-t}\,dt$ is the incomplete $\Gamma$ function. The characteristic slowest relaxation rate in the model (associated with the slowest relaxation mode of characteristic chains) is given by $\epsilon_{char} = \epsilon_x(N_x/N_{char})^{2/d_R}$. Since the spectrum of relaxation modes is cutoff at $\epsilon = \epsilon_x$ in our model, $G_x = ckT/N_x$ where $c$ is the number density of monomers, $k$ is the Boltzmann constant and $T$ is the absolute temperature.

For HBP melts with branch length $N_x$, we showed previously[14] that chains are strongly overlapped with fractal dimension $d_f = 4$ on mass scales $N < N_c$ and are marginally overlapped (i.e., in a quasi-$c^*$ state) with fractal dimension $d_f = 3$ on mass scales $N > N_c$, where $N_c$ is a crossover mass that scales as $N_c \cong N_x^3$. Since $N_x = 2P_x \approx 10$ for the H10 series (see Table 6), $N_c \approx 1000$ so that for all the samples in the H10 series, the polymer chains are strongly overlapped over most relevant mass scales (i.e., $d_f = 4$). Cates[38] has shown that for randomly branched chains which are strongly overlapped, hydrodynamic interactions are fully screened. Since we assume that chains in the H10 series are unentangled, the relevant dynamics governing chain relaxations is Rouse dynamics where the dimension of the relaxation rate spectrum is given by[37]

$$\frac{d_R}{2} = \frac{d_f}{2+d_f} \quad (3)$$

Thus, when fitting rheology data for the H10 series using eq 2, we have two fitting parameters, namely $G_x$ and $\epsilon_x$.

As explained in our previous study,[17] in the limit $N_{char} \gg N_x$ (i.e., $a \ll 1$), eq 2 has the limiting behavior $G^*(\omega) \sim (i\omega)^{d_R/2}$ within the frequency range $\epsilon_{char} \ll \omega \ll \epsilon_x$, where $\epsilon_{char}$ is the characteristic slowest relaxation rate in the model. From this result, it immediately follows that $\tan\delta \equiv G''/G' = \tan \pi d_R/4$ in the frequency range $\epsilon_{char} \ll \omega \ll \epsilon_x$, where $\delta$ is the phase angle measured by rheology. These results are in contrast to polymer gels ($\tau > 2$)[37] where the corresponding results in the scaling regime are $G^*(\omega) \sim (i\omega)^{d_R(\tau-1)/2}$ and $\tan\delta \equiv G''/G' = \tan \pi d_R(\tau-1)/4$, respectively. In principle therefore, we can determine the dimension of the relaxation rate spectrum $d_R$ by measuring the slope of the dynamic moduli or the value of $\tan\delta$ in the scaling regime.

However as we shall see in section 4.4, the values of $N_{char}$ required to obtain pure power law behavior at intermediate frequencies turn out to be extremely large so that for HBPs, this dynamic scaling regime is unattainable in practice. The actual value of $d_R$ can therefore only be inferred indirectly by fitting to the dynamic moduli data over the entire frequency range. The situation here is again in contrast to polymer gels where because of the existence of a gel point, arbitrarily large values of $N_{char}$ can be obtained (by going arbitrarily close to the gel point), so that a pure scaling regime is achievable. One can therefore measure $d_R$ (or more strictly $d_R(\tau-1)/2$) directly for polymer gel systems.[5,37,39,40]

**3.2.2. Entangled Regime.** For the H1 series we have $N_x > N_e$. We therefore assume that the HBP chains are entangled and model the rheology using the tube model. This is a formidable task given that the HBP ensemble is a complex mixture of linear and branched molecules of varying degrees of branching.

To aid us in this task, we first recognize that the linear rheology of any branched ensemble is determined by the "seniority" distribution of its spacers[11,41] (we define a spacer as a chain portion between branch points). The seniority $m$ of a spacer is defined as the number of spacers (including the spacer in question) connecting it to the retracting chain end responsible for its relaxation. As such, $m$ characterizes the "depth" of the spacer from the topological exterior of the molecule to which it belongs. The full seniority distribution for branched polymers in the mean field HBP class has been calculated by Read and McLeish.[11] However for the H1 series, we shall only require the concentration of $m = 1$ spacers. This is because for this series, the relatively low values of $b_U$ and $N_x$ mean that by the time the $m = 1$ spacers have relaxed, the "dynamically diluted" tube diameter is larger than the spacer length so that one expects the entire sample to become disentangled. (In fact, as we shall see in section 4.5, in a more refined tube model, one should include branch length renormalization under dynamic dilution which would delay disentanglement.)

Milner and McLeish[42] have shown that for star-linear blends, the reptation of linear species leads to constraint-release Rouse motion of the tubes constraining the star arms which is not described by dynamic dilution. Since we have a significant fraction of linear species in the H1 series, for seniority $m = 1$ spacers, we explicitly distinguish between linear spacers and terminal spacers (for metallocene systems, a similar calculation has been performed by Costeaux and Wood-Adams).[43] Specifically a spacer is linear when it is unbranched in *both* the upstream and downstream direction. The volume fraction of linears is therefore given by

$$\phi_l = (1-b_U)(1-b_D) \quad (4)$$

where $b_D = 2b_U$ is the downstream branching probability.[11] (The result $b_D = 2b_U$ can be readily understood as follows. In the absence of loops, the total number of strands which hit a branch point downstream is twice the number of strands which hit a branch point upstream, since each (trifunctional) branch point has two strands hitting it in the down stream direction but only one strand hitting it in the upstream direction. This immediately yields $b_U = 2b_D$.) On the other hand, a spacer is terminal if it is unbranched in the upstream direction and it is branched in the downstream direction, *or* it is branched in the upstream direction and it is unbranched in the downstream direction. The volume fraction of terminal spacers is therefore given by

$$\phi_t = b_U(1-b_D) + b_D(1-b_U) \quad (5)$$

Finally we refer to all remaining spacers (which have seniority 2 or higher) as internal spacers and these have volume fraction

$$\phi_i = 1 - \phi_l - \phi_t = b_U b_D \quad (6)$$

Having distinguished between the different spacers in the ensemble, we then developed a tube model that incorporates chain relaxation mechanisms such as reptation (for the linear species) and arm retraction as well as tube relaxation mechanisms such as dynamic dilution and constraint-release Rouse motion. Details of the tube model are given in appendix *A* and

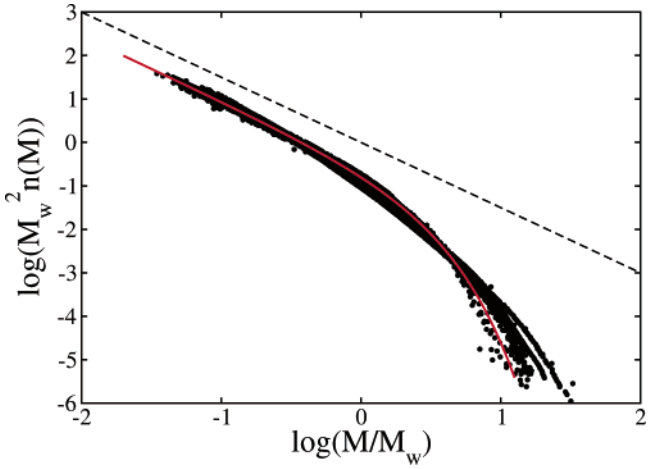


**Figure 3.** Universal plot for the number density of the H10 series. Symbols represent experimental data. The solid line is the best fit to the data using the functional form $AM^{-\tau}\exp(-BM/M_w)$ (assuming $\tau = 1.5$). The dashed line represents a slope of 1.5 as guide to the eye.

the final result for the dynamic moduli is given by eq 35. This equation contains three fitting parameters, namely $G_e$, $N_e$, and $\tau_e$, which are the entanglement modulus, spacing, and Rouse time, respectively.

## 4. Results and Discussion

**4.1. Size Exclusion Chromatography.** The number density for H10 was determined from the DRI and the 15° LS signal of the triple detector using[25,44]

$$n(M_i) = -\frac{M_0}{2.303M_i^2}\frac{c_i}{c}\frac{dV_i}{d(\log M_i)} \quad (7)$$

where $M_0$ is the (mole averaged) molecular weight of the AB and $AB_2$ monomers, $c$ is the area under the DRI chromatogram, $M_i$ and $c_i/c$ are respectively the weight-average molecular weight and weight fraction of polymer in the $i$th elution volume. The derivative $dV_i/d(\log(M_i))$ was obtained by performing a cubic fit to the $\log(M)$ vs $V$ plot for a particular column calibration by superposing several runs for different samples.

For HBPs, $M_{char}$ is proportional to $M_w$ in the limit $M_{char} \gg M_x$.[17,25] If this proportionality applies, it should be possible to construct a universal curve for the number density by plotting $M_w^2 n(M)$ vs $M/M_w$.[25,45] In Figure 3, we construct such a universal plot for the H10 series. Fitting the universal curve to the functional form $AM^{-\tau}\exp(-BM/M_w)$ (assuming $\tau = 1.5$ and using $A$, $B$ as fitting parameters), the best fit to the data (solid line) is obtained for $M_{char}/M_w \approx 1.7$, where in this context $M_{char}/M_w = B^{-1}$. However we note that the collapse of the data is relatively poor, with systematic deviations appearing at high molecular weights. The assumed functional form also underpredicts the universal curve at the high molecular weight end.

Since we require an accurate parametrization of the MWD to model the H10 rheology (see section 3.3.1), we decided to fit the MWDs for each individual sample separately using eq 1 (again assuming $\tau = 1.5$). The resultant fits are shown in Figure 4 and the fitted values of $M_{char}$ for each sample are reported in Table 4. From Figure 4, we see that this procedure produces much better fits to the H10 MWD data (though there are still small deviations for H10-256). From Table 4, we see that the ratio $M_{char}/M_w$ is not constant across the H10 series but increases systematically by about 50% with increasing molecular weight. This explains why the collapse of the number density data with $M_w$ in Figure 3 was relatively poor.

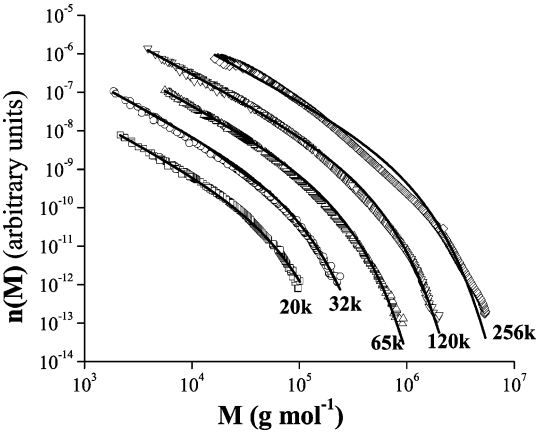


**Figure 4.** Fits to MWDs for each individual sample in the H10 series using eq 1 (assuming $\tau = 1.5$). For the sake of clarity, vertical shifts of 10, $10^2$, $10^3$, and $10^4$ have been applied to the curves for H10-32, H10-65, H10-120, and H10-256, respectively.

**Table 4. Fitted values of $M_{char}$ for the H10 series obtained from the fitting in Figure 4**

| sample | $M_w$ | $M_{char}$ | $M_{char}/M_w$ |
|---|---|---|---|
| H10-20 | 20300 | 33100 | 1.63 |
| H10-32 | 31900 | 52700 | 1.65 |
| H10-65 | 64500 | 123900 | 1.92 |
| H10-120 | 119900 | 264200 | 2.2 |
| H10-256 | 256100 | 650000 | 2.54 |

As we have explained at the beginning of this section, $M_{char}/M_w$ is only constant in the asymptotic limit $M_{char} \gg M_x$. For HBPs with trifunctional branch points, the actual value for this ratio is predicted by mean field theory to be $M_{char}/M_w = 1/(1 - 2b_U^2)$ (see eqs 6.21, 6.30, and 6.31 in ref 44, using $f = 3$ and recognizing that $b_U$ plays the role of $p$ in these equations). Thus, $M_{char}/M_w$ is not constant except when we are very close to the mean field gel point of $b_U = 0.5$. For the $b_U$ values for H10 quoted in Table 6, we obtain an increase in $M_{char}/M_w$ of about 20% going from the lowest to the highest molecular weight samples. This variation is lower than but of the same order of magnitude as the 50% variation seen in Table 4. Mean field theory also predicts that the maximum value of $M_{char}/M_w$ is $M_{char}/M_w = 2$ (for $b_U = 0.5$). However for the two highest molecular weight samples in Table 4, we find $M_{char}/M_w > 2$. We speculate that this may be due to residual fluctuation effects in the H10 series, which we expect to be strongest for the highest molecular weight samples.

Interestingly, in a previous study of HBP samples with similar chemistry but shorter spacer lengths,[25,46] we also encountered problems when constructing universal curves for the number density using $M_w$. Specifically we found that for the highest molecular weight sample studied ($M_w \approx 250$K g/mol), there was poor collapse of the number density onto the universal curve. In that study, we attributed the poor collapse to the fact that the largest molecules in the high molecular weight sample had exceeded the exclusion limit of the SEC columns (this would result in a poor resolution of the high molecular weight tail and consequently an inaccurate determination of the number density). However in the light of our discussion in the previous paragraph, an alternative explanation may be that $M_{char}/M_w$ was not in fact constant across the series because the samples in the series were also not close enough to the mean field gel point to achieve the asymptotic limit of constant $M_{char}/M_w$.

**4.2. Determination of Rate Constants from Reaction Kinetics Model.** In this section, we determine the rate constants for the different functional groups in the system by fitting the

**Table 5. Comparison of Average $A_IB_J$ Concentrations Determined from NMR with Predictions of the Reaction Kinetics Model for Different Values of the Ratios $k_M/k_P$ and $k_T/k_P$**

| | NMR | $k_M/k_P = 1$, $k_T/k_P = 1$ | $k_M/k_P = 0.8$, $k_T/k_P = 3$ | $k_M/k_P = 1$, $k_T/k_P = 0.5$ |
|---|---|---|---|---|
| TT | $3.7 \pm 0.6$ | 3.2 | 3.7 | 2.7 |
| TM | $5.7 \pm 0.3$ | 5.5 | 5.0 | 5.8 |
| TP | $4.0 \pm 0.3$ | 4.8 | 4.8 | 5.1 |
| MT | $12.4 \pm 0.5$ | 11.0 | 12.7 | 9.0 |
| PT + MM | $28.5 \pm 0.5$ | 28.4 | 28.3 | 27.7 |
| MP | $16.7 \pm 0.6$ | 16.4 | 16.3 | 17.3 |
| PM | $15.4 \pm 0.6$ | 16.4 | 15.0 | 17.3 |
| PP | $13.6 \pm 0.6$ | 14.3 | 14.2 | 15.1 |

relative concentrations of reacted bonds of type $A_IB_J$ (I, J = P, M, or T) in the H10 series (as measured by NMR) using the reaction kinetics model (where $A_IB_J$ is equivalent to IJ in the notation of Table 3 and Figure 2).

We first assumed that all A groups behave identically, but that B groups on different monomers react at different rates $k_P$, $k_M$, and $k_T$, which we attempt to determine (further details of this model are given in Supporting Information). In principle, the relative concentrations of reacted bonds of type $A_IB_J$ for the different samples contain information that could be used to deduce the reaction rate constants. For an individual sample, with known $f_M$, $f_P$, and $f_T$, one might envisage varying the ratios $k_M/k_P$ and, while using the reaction probability to match the sample molecular weight, to "best fit" the $A_IB_J$ concentrations. Unfortunately, there is significant scatter from sample to sample in the $A_IB_J$ concentration data, so that it is difficult to be confident of ratios $k_M/k_P$ and $k_T/k_P$ obtained from fitting individual sample data.

An alternative strategy is suggested by the observation that, at fixed $k_M/k_P$ and $k_T/k_P$, the $A_IB_J$ concentrations predicted by the reaction kinetics model are practically independent of the sample molecular weight across the range of molecular weights covered by the samples. On this basis, it is reasonable to take an average of the $A_IB_J$ concentrations across the samples (even though they have different molecular weights), and to compare these averaged concentrations with the reaction kinetics model. The intention here is to check whether, taken as a whole, the $A_IB_J$ concentrations across the H10 samples suggest any trends in the ratios $k_M/k_P$ and $k_T/k_P$.

Table 5 shows the average $A_IB_J$ concentrations, with the errors given by $\sigma/\sqrt{5}$, where $\sigma$ is the standard deviation of the data for a given reaction bond type across all the samples. The table also shows predictions of the reaction kinetics model for different values of the ratios $k_M/k_P$ and $k_T/k_P$. These are calculated at monomer fractions $f_M = 0.462$, $f_P = 0.403$, and $f_T = 0.135$, which are values obtained by averaging NMR results over all the samples. From the table, it can be seen that, in fact, the assumption of equal reaction rates ($k_M/k_P$ and $k_T/k_P = 1$) does a reasonable job of describing the data. Some improvements are obtained by increasing the relative rate of reaction of the B groups on the trivalent T monomer ($k_T/k_P = 3$) and by slightly decreasing the relative reactivity of the B groups on the M monomer ($k_M/k_P = 0.8$), though the improvements are largely within the range of experimental noise. Note that, with these changes, practically all the B groups on the trivalent T monomer react, so that further increases in $k_T/k_P$ have little effect (predictions with, for example, $k_T/k_P = 10$ are indistinguishable). On the other hand, decreasing $k_T/k_P$ has a much more significant effect on the data, specifically worsening the agreement between theory and experiment. This is illustrated in Table 5 for $k_M/k_P = 1$, $k_T/k_P = 0.5$ where we see that there are now significant deviations between the reaction kinetics model and the NMR data (especially for TT, MT, PM, and PP). Therefore, while our analysis of the NMR data does not allow us to determine the reactive constants very accurately, it does show fairly conclusively that the B-groups on the T monomer are more reactive than those on the P and M monomers.

**Table 6. Output of reaction kinetics model for H10 and H1 series**

| | $k_M/k_P = 1$, $k_T/k_P = 1$ | $k_M/k_P = 0.8$, $k_T/k_P = 3$ |
|---|---|---|
| H10-20 | $b_U = 0.397$, $P_x = 4.3$ | $b_U = 0.412$, $P_x = 3.2$ |
| H10-256 | $b_U = 0.473$, $P_x = 3.9$ | $b_U = 0.477$, $P_x = 2.9$ |
| H1-18 | $b_U = 0.225$, $P_x = 22.0$ | $b_U = 0.232$, $P_x = 21.2$ |
| H1-43 | $b_U = 0.304$, $P_x = 29.0$ | $b_U = 0.308$, $P_x = 28.0$ |
| H1-63 | $b_U = 0.356$, $P_x = 25.0$ | $b_U = 0.359$, $P_x = 24.0$ |
| H1-76 | $b_U = 0.367$, $P_x = 25.8$ | $b_U = 0.371$, $P_x = 24.7$ |

Using a similar approach, we also investigated the assumption that the A groups on the three monomers possess different reactivities, while keeping the B group reactivities identical (see Supporting Information for further details). Using this alternative assumption, it was possible to obtain slight improvement in the description of the $A_IB_J$ concentration as compared to the limit of equal reactivities, although the improvement was not so marked as in the above case of different B group reactivities.

In summary, the NMR data on the H10 series are suggestive of some relatively small variations in group reactivity from monomer to monomer. In particular, they suggest that the B groups on the T monomer are more reactive than those on the P and M monomers.

**4.3. $b_U$ and $P_x$ from the Reaction Kinetics Modeling.** In this section, we determine the upstream branching probability $b_U$ and average branch length $P_x$ from the rate constants determined in the previous section (further details of the calculation are given in Supporting Information). Table 6 shows values of $b_U$ and $P_x$ calculated for the highest and lowest molecular weight samples from the H10 series, using both $k_M/k_P = 1$, $k_T/k_P = 1$ and $k_M/k_P = 0.8$, $k_T/k_P = 3$. Note that for the H10 series, the variation in rate constants of the different functional groups has a significant effect on the predicted branch length $P_x$. However in the unentangled regime, the rheology is only weakly dependent on the branch length so that this level of uncertainty in $P_x$ is not a cause for concern for the rheological modeling. More importantly, both sets of monomer reactivities predict that the effective branch length of all the samples in the H10 series fall below the entanglement spacing, i.e., $N_x = 2P_x \approx 10$ while $N_e \approx 15$ (see section 4.5).

Table 6 also shows values of $b_U$ and $P_x$ calculated for the samples from the H1 series, using both $k_M/k_P = 1$, $k_T/k_P = 1$ and $k_M/k_P = 0.8$, $k_T/k_P = 3$. Here the effective branch length $N_x = 2P_x$ is above the entanglement degree of polymerization in all cases. Note that for the H1 series, the variation in the rate constants of the different functional groups has only a mild effect on both $b_U$ and $P_x$. This is largely because, even with $k_M/k_P = 1$, $k_T/k_P = 1$, most of the B units on the trifunctional monomers have reacted, so that the vast majority of these monomers give rise to a branch point. An increase in their reactivity ($k_T/k_P = 3$) has only a mild effect on the predicted parameters $b_U$ and $P_x$ (whereas a decrease to $k_T/k_P < 1$ has a stronger effect). For this reason, it is important to note that the NMR data on the H10 series are most consistent with $k_T/k_P > 1$. Using a similar approach, we also investigated the assumption that the A groups on the three monomers possess different reactivities, while keeping the B group reactivities identical (see Supporting Information). With this alternative assumption, it remains the case that predictions for $b_U$ and $P_x$ for the H1 series appear to be insensitive toward variations in reactivity of the A units within the range consistent with the H10 NMR data.

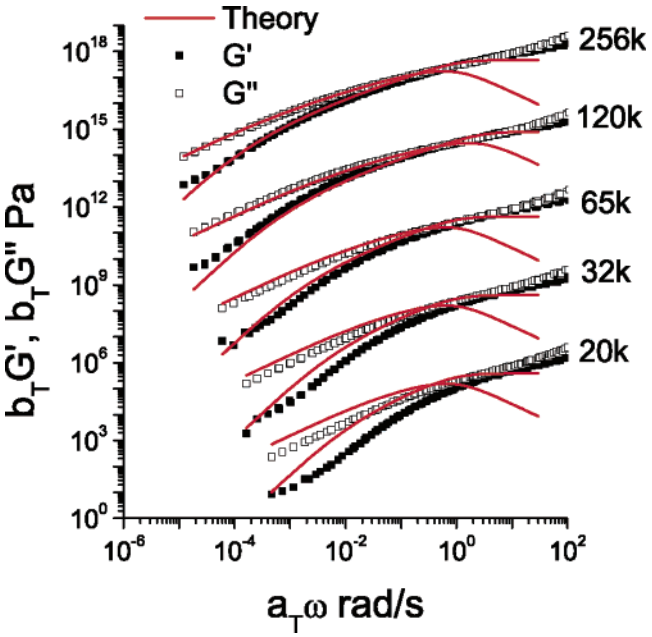


**Figure 5.** Fits to the rheology of the H10 series using the dynamic scaling model (i.e., eqs 2 and 3). Symbols represent experimental data and solid lines the best fits. The data for H10-32, H10-65, H10-120, and H10-256 have been shifted vertically by factors of $10^3$, $10^6$, $10^9$, and $10^{12}$ respectively for clarity.

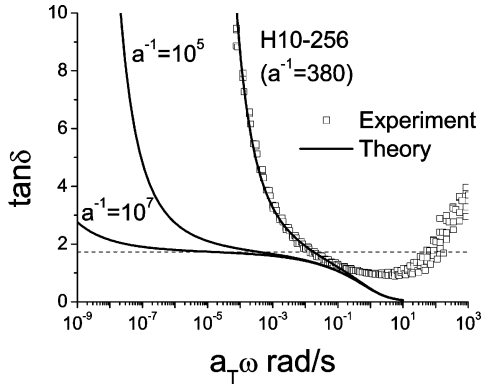


**Figure 6.** tan $\delta$ for H10-256 ($N_{char}/N_x = a^{-1} = 380$) and the dynamic scaling predictions for $\epsilon_x = 1.4$ rad/s and $N_{char}/N_x = a^{-1} = 380$, $10^5$, and $10^7$ (solid lines). We also show the limiting value of tan $\delta$ in the scaling regime, i.e., tan $\delta$ = tan $\pi d_R/4 = 1.73$ (dashed line).

In summary, for the H1 series, the values for $b_U$ and $P_x$ reported in Table 6 are robust with respect to reasonable variations in microscopic details of the reaction kinetics model. We therefore expect the uncertainties in the parameters $b_U$ and $P_x$ for the H1 to be small, for example as compared to uncertainties in the entanglement molecular weight for this polymer chemistry.

**4.4. Rheology of H10.** Figure 5 shows the rheology results for the H10 series (data files for the rheology can be obtained from Supporting Information). For each sample, we used a reference temperature of $T_g + 21 \pm 2$ °C and this superposed the high-frequency region for the mastercurves of all the samples. The high-frequency regime corresponds to the glassy regime as evidenced by the breakdown of time−temperature superposition (see Figure 6). The superposition of all the mastercurves at high frequency indicates that we have effectively normalized the monomeric friction coefficient for all the samples to a common value. The features of the rheology data are similar to those of unentangled HBP samples that we have studied previously.[17,25,47] In particular, we note that for all our samples, there is no crossover in $G'$ and $G''$ at low frequencies. This indicates that the HBP chains are unentangled, independent of molecular weight, a fact that is confirmed by the detailed theoretical modeling in the rest of this section.

In Figure 5, we show fits to the $G'$, $G''$ data for all the samples using eqs 2 and 3. For all the samples, we used $\tau = 1.5$ and $M_{char}$ reported in Table 4. To obtain the fits, we first fitted the dynamic moduli of the highest molecular weight sample H10-256 using $\epsilon_x$ and $G_x$ as our fitting parameters. The best fit parameters were found to be $G_x = 5 \times 10^5$ Pa and $\epsilon_x = 1.4$ rad/s. The same fitting parameters were then used to predict the dynamic moduli for all the other samples. We note that the fitted value for $G_x$ has the correct order of magnitude compared to the value predicted by rubber elasticity theory, i.e., $\rho RT/M_x = 1.4 \times 10^6$ Pa (using $\rho = 1$ g/cm$^3$ and $M_x = 2P_xM_0 = 1700$ g/mol, where $P_x = 5$ is the number-average spacer length, $M_0 = 170$ g/mol is the mole averaged monomer weight). For the two samples with the highest molecular weight, H10-256 and H10-120, there is excellent agreement between theory and experiment over about four decades in frequency. The excellent agreement between the Rouse model and the experimental data confirms our earlier observation that these materials are unentangled.

The response at high frequencies is not predicted well by our dynamic scaling model (for all samples in the H10 series) because we have neglected relaxation modes with $\epsilon > \epsilon_x$ in our model. Fits to the high frequency regime can be improved by explicitly including these glassy modes.[48,49] From Figure 5 we also see that for all samples in the H10 series, there appears to be a small but systematic upward curvature in $G'$ at the lowest frequencies. For H10-256 and H10-120, where the dynamic scaling model is most accurate, we see that this upward curvature in $G'$ is not captured by the dynamic scaling model. The maximum phase angles in this low-frequency regime range from 85 to 89° depending on the sample. Although high, these values of $\delta$ lie within the range where the phase angle resolution of the rheometer is not a problem. We therefore believe that these low-frequency features are real and indicate the presence of slow modes not captured by the dynamic scaling model. Similar slow modes have been observed in hyperstar polymers[50−52] and other HBP system[53] and have been attributed to structural rearrangements of whole molecules. However given the limited frequency range of these features in our samples, we have not analyzed these slow modes in any further detail.

As discussed in section 3.3.1, in the limit $N_{char} \gg N_x$, the dynamic moduli should in principle shows pure power law behavior at intermediate frequencies ($\epsilon_{char} \ll \omega \ll \epsilon_x$) which would allow us to determine the dimension of the relaxation rate spectrum $d_R$ directly. However the value of $N_{char}$ required to access this scaling regime turns out to be so high that it is unattainable in practice for HBPs. This can be seen in Figure 6 where we plot tan $\delta$ for H10-256 ($N_{char}/N_x = a^{-1} = 380$) and the dynamic scaling predictions for $\epsilon_x = 1.4$ rad/s and $N_{char}/N_x = a^{-1} = 380$, $10^5$, and $10^7$ (solid lines), assuming eq 3 and $d_f = 4$. We also show the limiting value of tan $\delta$ in the scaling regime, i.e., tan $\delta$ = tan $\pi d_R/4 = 1.73$ (dashed line). From Figure 6, we see that even for our highest molecular weight sample $N_{char}/N_x = a^{-1} = 380$, a pure scaling regime does not exist. Indeed we need to go to $N_{char}/N_x = 10^7$ before we see the emergence of a pure scaling regime. These ultrahigh values of $N_{char}$ are clearly not achievable for HBPs.

The difficulty seems to stem from the extremely long-range effect (in frequency space) exerted by both the high and low-frequency cutoffs. For example for $N_{char}/N_x = 10^7$ in Figure 6,

$\epsilon_x = 1.4$ rad/s and $\epsilon_{char} = \epsilon_x(N_x/N_{char})^{2/d_R} = 4 \times 10^{-11}$ rad/s. However the scaling regime only exists in the narrow frequency range $10^{-6}$ rad/s $\lesssim\omega\lesssim 10^{-4}$ rad/s. This means that the effects of the cutoff function persist for over four decades in frequency below the upper cutoff frequency and above the lower cutoff frequency. For this reason, we need to have $\epsilon_x/\epsilon_{char} > 10^9$, i.e., $N_{char}/N_x > 10^6$ before we can see a scaling regime. Clearly the separation between the high and low cutoff frequencies are too small for all the samples in the H10 series for this to happen ($\epsilon_x/\epsilon_{char} = 3$ and 7500, respectively, for H10-20 and H10-256). As a consequence of this, we can only infer the value of $d_R$ indirectly by fitting to the dynamic moduli data over the entire frequency range. Unfortunately, as pointed out in our previous study,[17] the dynamic moduli are rather insensitive to reasonable variations in $d_R$. Therefore, although our assumed value of $d_R$ produces excellent fits to the H10-256 data in Figure 6, the data do not in fact allow us to determine $d_R$ accurately.

Returning to Figure 5, we see that for high molecular weight HBPs, there is good agreement between the dynamic scaling model and the experimental data (except at the highest and lowest frequencies for reasons already discussed above). However as we go to lower molecular weights, an increasing discrepancy between theory and experiment appears. This is perhaps not surprising since we expect dynamic scaling to breakdown at lower molecular weights because there is no longer a wide enough power law regime in the relaxation rate spectra (e.g., for H10-20, $\epsilon_x/\epsilon_{char} = 3$). Note that unlike in our previous studies,[17,25,47] we have not allowed $G_x$ or $\epsilon_x$ to vary across the different samples since the branch lengths are essentially the same and in the current study, we have been careful to normalize the monomeric friction coefficients across the different samples. Notwithstanding this discrepancy, the absence of a crossover in the experimental $G'$, $G''$ data clearly indicates that these low molecular weight materials are also unentangled.

An alternative approach to handling the discrepancy for the low molecular weight materials is to assume that hydrodynamic interactions may not be fully screened and the degree of hydrodynamic screening may vary with molecular weight. This introduces an additional fitting parameter into the dynamic scaling theory (a hydrodynamic screening exponent[49]), which may allow us to obtain better fits to the lower molecular weight materials. However, in this case, it is not clear whether the better fits would merely be due to the fact that we have an extra fitting parameter or because there is truly a change in the degree of hydrodynamic screening. As we have already discussed earlier in this section, since we are far from a true scaling regime, our experimental data do not allow us to distinguish between reasonable variations in $d_R$ and hence variations in the degree of hydrodynamic screening. In any case, as we have already mentioned earlier, it is questionable whether dynamic scaling still applies for our lowest molecular weight samples. Extending the dynamic scaling theory to include an additional hydrodynamic screening parameter may not therefore be physically very meaningful. We note that there have been a few attempts to study the transition from Rouse to Zimm dynamics with molecular weight for both linear systems[54] and hyperbranched systems,[53] but the results have been inconclusive. Given that our aim here is to explain the data using the most economical model, we have opted to use the Rouse model to model the rheology of the H10 materials.

In summary, the experimental data and theoretical modeling above clearly show that HBP chains in the H10 series are unentangled regardless of molecular weight. We note that this finding is consistent with the study of Dorgan et al.[53] on a series of hyperbranched polystyrenes where $M_x < M_e$ (the highest $M_x$ used in this study was $M_x \approx 10\,000$ g/mol compared to $M_e \approx 13\,000$ g/mol for PS[2]). These authors were able to prepare polystyrene HBPs with weight-average molecular weights over $10^6$ g/mol, and remarkably, no entanglements were observed even at these extremely high molecular weights (though we note that $M_w/M_e \approx 100$ for these samples so that our highest molecular weight sample essentially has the same value of $M_w/M_e$). Our finding is also consistent with the study of Colby and co-workers[4–6] where they found that in the short branch length regime ($N_x < N_e$), the dynamic properties of randomly branched polymers in the percolation class are well described by the Rouse model for unentangled chains.

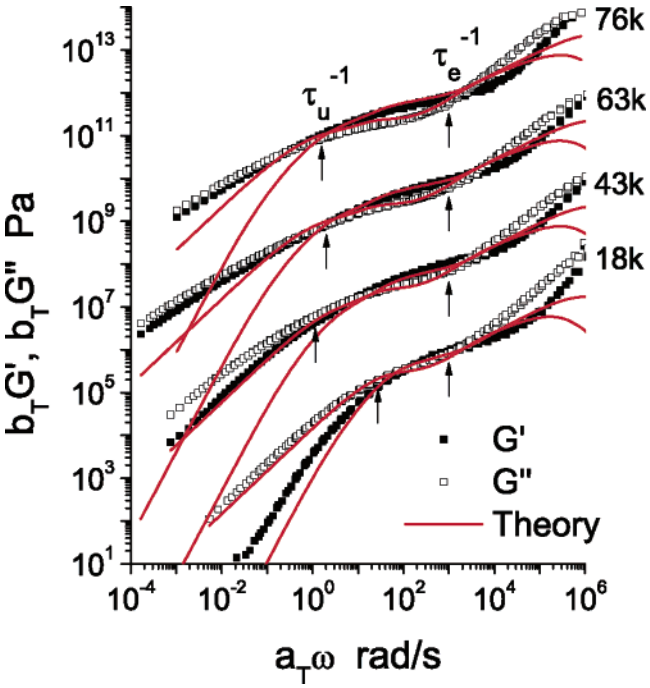


**Figure 7.** Fits to the rheology of the H1 series using eq 35. Symbols represent experimental data and solid lines the best fits. The data for H1-43, H1-63, and H1-76 have been shifted vertically by factors of $10^2$, $10^4$, and $10^6$, respectively, for clarity.

**4.5. Rheology of H1.** Fig. 7 shows the rheology results for the H1 series (data files for the rheology can be obtained from Supporting Information). For each sample, we used a reference temperature of $T_g + 38.5 \pm 4$ °C, and this superposed the high frequency (glassy) region for the mastercurves of all the samples. This indicates that we have effectively normalized the monomeric friction coefficient for all the samples to a common value. Unlike the H10 series, a rubbery plateau is evident at intermediate frequencies for the three highest molecular weight samples, indicating the presence of entanglements. The presence of entanglements is confirmed by the detailed theoretical modeling in the rest of this section.

Note that entanglements also slow chain relaxations to the extent that for the higher molecular weight samples, we do not observe classical terminal scaling at frequencies below the rubbery plateau. Instead, with increasing molecular weight, $G'$ and $G''$ increasingly tend toward a power law form. In the detailed modeling that follows, we show that the rubbery plateau is primarily due to the relaxation of linear chains and terminal spacers while the slow modes at low frequency appear to be due to the relaxation of topologically deeper internal spacers.

To model the H1 rheology, we use the tube model described in Appendix A. In Figure 7, we show fits to the rheology data

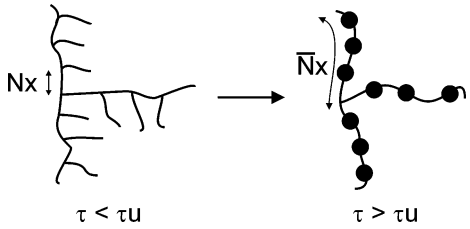


**Figure 8.** Renormalization of the branch length of a highly branched species under dynamic dilution.

using eq 35 with $N_e$, $\tau_e$, and $G_e$ as our fitting parameters, which are the entanglement length, Rouse time and modulus respectively (see appendix A for the definition we use for these quantities). The dynamic dilution exponent is set to $\alpha = {}^4/_3$ as suggested by Colby and Rubinstein.[55] In principle, $N_e$ and $\tau_e$ can be determined from our rheological measurements of linear chain melts of the same chemistry while $G_e$ is related to $N_e$ via eq 12. In practice, however, it is difficult to obtain precise values for $\tau_e$ and $N_e$ from our rather low molecular weight, polydisperse linear samples (see section 2.5). In addition, constraining $G_e$ and $N_e$ to be related to each other via eq 12 often produces poor fits to rheological data.[28] We therefore use $\tau_e$, $N_e$, and $G_e$ as independent fitting parameters and then show that the values obtained are consistent with values obtained from measurements on linear chains and with eq 12.

We first fitted the dynamic moduli of the highest molecular weight sample H1-76 at intermediate frequencies (where $G'$ and $G''$ have the most distinctive features) and the best fit parameters obtained were $G_e = 1.2 \times 10^6$ Pa, $\tau_e = 10^{-3}$ s, and $N_e = 15.5$. Note that $G_e$ and $\tau_e$ control the modulus and frequency scale respectively, while $N_e$ controls the shape of the dynamic moduli, so the fitting parameters are fairly tightly constrained by the experimental data. The fitted value for $N_e$ is in excellent agreement with the value $N_e \approx 15$ obtained from fitting to the rheology of the linear samples. The fitted value of $G_e$ is also in excellent agreement with the value calculated from eq 12, i.e., $G_e = ckT/N_e \approx 1.2 \times 10^6$ Pa, where the number density of monomers is calculated from $c = \rho N_A/m_0$, where $N_A$ is Avogadro's number, $\rho = 1$ g/cm$^3$ is the approximate mass density of the HBP, $m_0 = 164$ g/mol is the monomer weight, and $T = 367$ K is the reference temperature we use for H1-76.

The values for $G_e$, $\tau_e$, and $N_e$ obtained from fitting H1-76 were then used to predict the dynamic moduli for all lower molecular weight samples without further fitting. We see that there is excellent agreement between theory and experiment in the rubbery plateau region between $\tau_u^{-1} < \omega < \tau_e^{-1}$, where $\tau_u$ is the disentanglement time defined by eq 32. In particular, the tube model predicts the narrowing and eventual disappearance of the rubbery plateau with decreasing molecular weight reasonably well. However for all the H1 samples, our tube model predicts a premature transition to terminal scaling for $G'$ and $G''$. Evidently the disentanglement criterion embodied in eq 32 (i.e., HBP chains become unentangled when the dynamically diluted entanglement length becomes greater than the undiluted branch length) is too strong. In fact, the assumption is strictly speaking incorrect because it neglects the fact that *branch lengths* are also renormalized under dynamic dilution.

What we mean is illustrated in Figure 8. At short times ($t < \tau_u$), a highly branched species has the undiluted branch length $N_x$. However at long times ($t > \tau_u$), the low seniority branches relax and act effectively as frictional beads. This process invariably leads to a longer effective spacer length $N_x(\Phi)$ for the "snipped" branch molecules. Thus, for $t > \tau_u$, the snipped molecules can still be entangled with each other so long as $N_x(\Phi)$ grows fast enough to satisfy the condition $N_x(\Phi) > N_e(\Phi)$. It would appear that this process of branch length renormalization is nonnegligible in our samples and is presumably what gives rise to the slow relaxations observed in our experiments. We note that branch length renormalization has been incorporated into an algorithm devised by Larson[56] for calculating the rheology of polydisperse melts containing linears, stars and combs. This algorithm can be generalized to handle more highly branched samples such as our HBP melts,[36] but to do so lies beyond the scope of this paper.

Notwithstanding the discrepancy at low frequencies, our tube model quantitatively confirms that the HBP chains in the H1 series are entangled. Taking the results for H1 ($N_x > N_e$) and H10 ($N_x < N_e$) together, we therefore conclude that for randomly branched polymers in the HBP class, the entanglement transition is controlled by the branch length $N_x$ and the transition occurs around $N_x \approx N_e$. This is the same conclusion found by Colby and co-workers[4−6] for randomly branched polymers in the percolation class. In the next section, we explain this result using scaling theory.

## 5. Scaling Argument for the Entanglement Transition of Randomly Branched Polymers

Recall that for randomly branched polymers, the entanglement transition is controlled by $N_x$ and the transition occurs around $N_x \approx N_e$. For $N_x > N_e$, it is not surprising that branched polymers are entangled, since chain portions are linear on the mass scale of $N_e$ and we therefore expect the entanglement behavior to be essentially the same as linear polymers. For $N_x < N_e$, however, while it is clear that entanglements do not occur at the level of linear spacers, it is not at all clear why entanglements do not occur between branched sections on larger mass scales. Indeed, we[14] have shown that randomly branched polymers in the HBP and percolation class remain strongly overlapped up to the crossover mass of $N_c = N_x^3$ and $N_c = N_x^{5/3}$ respectively. Since $N_e$ can be rather large for some polymers, it is possible for $N_x$ to be simultaneously small enough to satisfy the condition $N_x < N_e$ and large enough for branched sections to be strongly overlapped to very high mass scales and hence potentially entangled.

To analyze this problem theoretically, we need to first consider the more general question of what constitutes an entanglement in polymeric systems. Unfortunately there is currently no microscopic model that answers this question satisfactorily, though there are a number of competing scaling theories (see refs 57 and 58 for excellent discussions of these scaling theories). The two most widely used scaling models are the double reptation model[59−61] and the Colby−Rubinstein model,[55] and it is to these models that we shall appeal in the following discussion.

**5.1. Scaling Models for Entanglements.** A central parameter to all the scaling models above is the so-called packing length $l_p \equiv v_0/b^2$ where $v_0$ is the effective monomer volume and $b$ is the effective monomer length. The packing length $l_p$ is thus a material specific parameter, and it defines the closest distance of approach between polymer chains of a given chemistry.[58] In terms of the packing length, the concentration of binary contacts for polymers chains of a given chemistry in a $\Theta$ solution with volume fraction $\phi$ is given by $c_B = \phi^2/l_p^3$.[58] This result follows from two facts. First, in a $\Theta$ solvent, there are no strong correlations between the different chains so that binary contacts between chains are random and therefore proportional to $\phi^2$. Second, for $\phi = 1$ (melt regime), $c_B = 1/l_p^3$ since $l_p$ defines the distance of closest approach between polymer chains.

In the Colby−Rubinstein model, an entanglement occurs when the number of binary contacts between different chains within the volume swept out by one of the chains is equal to a critical number $n_c$, which is presumed to be universal (i.e., independent of chemistry). Within the Colby−Rubinstein ansatz, the entanglement degree of polymerization $N_e$ for a Θ solution of linear chains with volume fraction $\phi$ is therefore given by

$$\frac{R(N_e)^3\phi^2}{l_p^3} = n_c \tag{8}$$

where $R(N)$ is the distance spanned by a chain of length $N$. Since $R(N) \sim N^{1/2}$, it follows that $N_e^{3/2}\phi^2 = \text{const}$, i.e., $N_e \sim \phi^{-4/3}$. Equation 8 also defines the tube diameter $a$ via $a = R(N_e)$.

In the double reptation model, an entanglement occurs when the number of binary contacts between a given chain and other chains is equal to a critical number $n'_c$ ($n'_c$ is again presumed to be universal). Now the volume fraction of monomers belonging to a given chain of mass $N$ within its own spanned volume is given by $\phi_{self} = Nv_0/R(N)^3$. For a Θ solution of polymer chains with volume fraction $\phi$, the concentration of binary contacts between a given chain and other chains is proportional to $\phi_{self}\phi/l_p^3$. Within the double reptation model, the entanglement degree of polymerization $N_e$ for a Θ solution of linear chains is therefore given by

$$\frac{R(N_e)^3\phi_{self}\phi}{l_p^3} = \frac{N_e v_0 \phi}{l_p^3} = n'_c \tag{9}$$

It follows that $N_e \sim \phi^{-1}$. The Colby−Rubinstein prediction of $N_e \sim \phi^{-4/3}$ turns out to be closer to the experimental data for linear chains in Θ solution[62] compared to the double reptation model. However in what follows, we shall analyze the entanglement transition of randomly branched polymers using both models.

Of course, for the problem at hand, we are interested in branched polymer *melts* not solutions. However we note that since the samples are polydisperse, there is a multiplicity of time scales in the system and on a given time scale, some of the material has already relaxed and acts as a Θ solvent for the rest of the unrelaxed material. Therefore, on any given time scale, we effectively have a Θ solution of unrelaxed material to which we can apply the above scaling theories to determine the entanglement weight.

**5.2. Fraction of Dynamically Relevant Material.** To determine the fraction of dynamically relevant material on any given time scale, we note that since we are interested in chain relaxations on the scale of an entanglement, the relevant dynamics are Rouse dynamics. Within Rouse dynamics, each time scale is associated with a mass scale so that time scales and mass scales are interchangeable, independent of whether chains are linear or branched (at least at the level of scaling theory). On time scales associated with a mass scale $N$, it is clear that *whole molecules* with mass less than $N$ are not able to entangle larger molecules since they have fully relaxed. However for molecules with mass greater $N$, it is also important to distinguish between *side branches* which have mass less than $N$ and remaining material which we define as *backbone* material. Since side branches smaller than $N$ are also able to explore all their internal configurations on the time scale of $N$, they are also not dynamically relevant in terms of entanglement formation. The only dynamically relevant material is therefore the "backbone" fraction of large chains.

For linear chains, the distinction between side branches and backbone is not critical since the fraction of side branches (i.e., free ends) is negligible in the limit of long linear chains. Our assumption that one should neglect the contribution from side branches when determining the entanglement mass therefore does not affect our earlier scaling results for linear chains.

To summarize, the procedure we take is as follows. For a given mass scale $N$, we first assess the number of relevant binary contacts between backbone material at that mass scale (using either a Rubinstein−Colby or double reptation argument). If, at some mass scale, the number of such contacts exceeds the critical value, we conclude entanglements are important at that mass scale. The smallest $N$ for which this is true defines $N_e$. To perform this analysis, we need to know the fraction of backbone material in a molecule at mass-scale $N$, which we now calculate.

For $N < N_x$, the fraction of dynamically relevant material $\phi \approx 1$ for both HBPs and percolation systems since at the level of our current scaling theory, we can neglect any polydispersity in the branch lengths. For $N > N_x$, we can estimate the backbone fraction $\phi$ that survives dynamic dilution as follows. For HBPs, we can choose a spacer at random and ask for the probability that the total molecular weight in the upstream direction is $N$. Because of the statistical self-similarity of the molecules, this is equivalent to choosing an unreacted A group at random, and asking for the probability distribution of the molecular weight of the molecule attached to it. There is one such A group per molecule, so this is the number distribution, as given in eq 1 and it scales as $N^{-3/2}$. If, on the other hand, we ask for the probability that the total molecular weight in the downstream direction is $N$, this is equivalent to choosing an unreacted B-group at random and asking for the probability distribution of the molecular weight. Since the number of unreacted B groups on a molecule is proportional to the mass of the molecule itself, this gives the weight-average molecular weight distribution, which scales as $N^{-1/2}$. Hence, for a randomly chosen spacer, the molecular weight in the downstream direction is usually large, and the "side branch" is usually upstream, having a molecular weight $N$ with probability scaling as $N^{-3/2}$. The probability that this randomly chosen spacer is part of a side branch *larger* than $N$ therefore scales as $\int_N^\infty N^{-3/2}\, dN \sim N^{-1/2}$. As we have said earlier, the spacer needs to be part of a side branch that is larger than $N$ to be effective at entangling, so $\phi \sim N^{-1/2}$.

For mean field percolation clusters, both directions are equivalent to the "upstream" direction of HBPs. Since one always takes the smaller molecular weight of the two directions, in order for a spacer to belong to a side branch larger than $N$, it needs to be part of a side branch larger than $N$ in *both* directions. The volume fraction of backbone material therefore scales as $\phi \sim N^{-1}$ for percolation clusters.

**5.3. Colby—Rubinstein Model.** We first analyze the entanglement transition of randomly branched chains using the Colby−Rubinstein model. We can apply eq 8 directly to this problem so long as we recognize that $\phi$ represents the fraction of dynamically relevant material and $R(N)$ has a different scaling with respect to $N$ depending on whether the chains are linear or branched on the mass scale of interest. Specifically, information regarding the degree of branching of the chains enters through the fractal dimension $d_f$ via $R(N) \sim N^{1/d_f}$. As we have already discussed, the value of $\phi$ depends on the time/mass scale of interest and branching statistics of the chain: For HBPs, $\phi \approx 1$ on mass scales $N < N_x$ while $\phi \sim N^{-1/2}$ on mass scales $N > N_x$. On the other hand, for percolation clusters, $\phi \approx 1$ on mass scales $N < N_x$ while $\phi \sim N^{-1}$ on mass scales $N > N_x$. In addition,

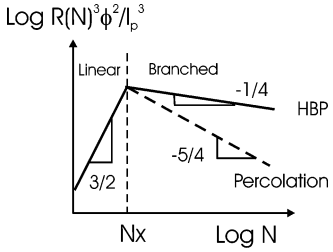


**Figure 9.** Number of dynamically relevant binary contacts within the volume spanned by the mass scale $N$ as a function of $N$ for HBPs (solid line) and percolation clusters (dashed line).

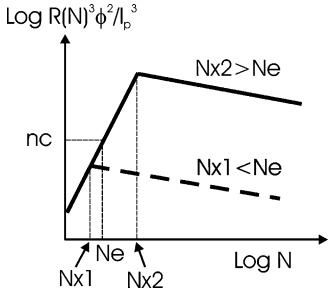


**Figure 10.** $R(N)^3\phi^2/l_p^3$ vs $N$ for HBPs for $N_x < N_e$ (dashed line) and $N_x > N_e$ (solid line). We also show the critical number of binary contacts needed to form an entanglement $n_c$ in the Colby−Rubinstein model, which corresponds to the entanglement mass $N_e$. For HBPs, $R(N)^3\phi^2/l_p^3 \sim N^{-1/4}$ for $N > N_x$. The corresponding plot for percolation clusters is similar except that $R(N)^3\phi^2/l_p^3 \sim N^{5-/4}$ for $N > N_x$.

since entanglements are believed to be a collective phenomenon due to many chains, it is implicitly assumed that we are in the regime where chains are strongly overlapped (i.e., $N < N_c$ for branched systems). Fractal dimensions are therefore given by their Gaussian values. For both HBPs and percolation clusters, we therefore have $d_f = 2$ on mass scales $N < N_x$ (since chains are linear on these mass scales) and $d_f = 4$ on mass scales $N > N_x$ (since chains are branched on these mass scales).

In Figure 9, we plot $R(N)^3\phi^2/l_p^3$, i.e., the number of dynamically relevant binary contacts (i.e., contacts between backbone material) within the volume spanned by the mass scale $N$, as a function of $N$ for HBPs (solid line). We also plot the analogous curve for percolation clusters (dashed line). For $N < N_x$, chains are linear and the number of binary contacts scales as $N^{3/2}$ for both HBPs and percolation clusters, i.e., the number of binary contacts *increases* with $N$. On the other hand for $N > N_x$, chains are branched and the number of binary contacts scales as $N^{-1/4}$ for HBPs and as $N^{-5/4}$ for percolation clusters, i.e., the number of binary contacts *decreases* with $N$. Consequently for both systems, the number of binary contacts is maximum for mass scales $N = N_x$.

In Figure 10, we plot $R(N)^3\phi^2/l_p^3$ vs $N$ for HBPs for both $N_x < N_e$ (dashed line) and $N_x > N_e$ (solid line). We also show the critical number of binary contacts needed to form an entanglement $n_c$ within the Colby−Rubinstein model (the intersection of $n_c$ with the increasing portion of the $R(N)^3\phi^2/l_p^3$ curve defines the entanglement degree of polymerization $N_e$). We see that for $N_x < N_e$, the maximum number of binary contacts always falls below the critical number required for entanglements. Thus, according to the Colby−Rubinstein model, HBP chains with $N_x < N_e$ are unentangled regardless of molecular weight. The analogous plot for percolation clusters is qualitatively the same except that $R(N)^3\phi^2/l_p^3 \sim N^{-5/4}$ for $N > N_x$ as we have already noted. Thus, the Colby−Rubinstein model predicts that percolation clusters with $N_x < N_e$ are also unentangled regardless of molecular weight. Both these predictions are in agreement with the experimental results in this paper and in the studies of Colby and co-workers.[4−6]

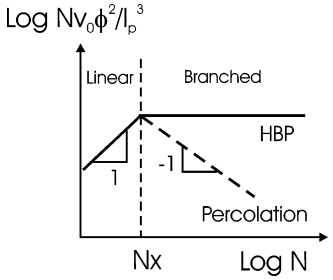


**Figure 11.** Number of dynamically relevant binary contacts between a given chain with original mass $N$ and other chains as a function of $N$ for HBPs (solid line) and percolation clusters (dashed line).

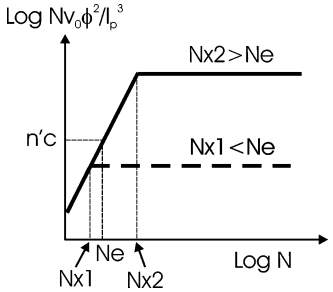


**Figure 12.** $N\upsilon_0\phi^2/l_p^3$ vs $N$ for HBPs for $N_x < N_e$ (dashed line) and $N_x > N_e$ (solid line). We also show the critical number of binary contacts needed to form an entanglement $n'_c$ in the double reptation model, which corresponds to the entanglement mass $N_e$. For HBPs, $R(N)^3\phi^2/l_p^3$ is constant with respect to $N$ for $N > N_x$. The corresponding plot for percolation clusters is similar except that $R(N)^3\phi^2/l_p^3 \sim N^{-1}$ for $N > N_x$.

**5.4. Double Reptation Model.** It turns out that we can also understand the entanglement transition for randomly branched polymers using the double reptation model and this is the approach we take in this section. Recall that in the double reptation model, an entanglement consists of a fixed number of binary contacts between a given chain and other chains. However in the case of randomly branched polymers, for a given chain with original mass $N$, the mass of the *dynamically relevant* fraction (i.e., the backbone) on time scales associated with $N$ is $N\phi$. The entanglement condition given by eq 9 should therefore be modified to

$$\frac{N_e \upsilon_0 \phi^2}{l_p^3} = n'_c \tag{10}$$

In Figure 11, we plot $N\upsilon_0\phi^2/l_p^3$, i.e., the number of dynamically relevant binary contacts between a given chain and other chains, as a function of the (original) mass of the chain $N$ for HBPs (solid line). We also plot the analogous curve for percolation clusters (dashed line). For $N < N_x$, chains are linear and the number of binary contacts scales as $N$ for both HBPs and percolation clusters, i.e., the number of binary contacts *increases* with $N$. On the other hand for $N > N_x$, chains are branched and the number of binary contacts is constant with respect to $N$ for HBPs and scales as $N^{-1}$ for percolation clusters. Consequently for both systems, the number of dynamically relevant binary contacts is maximum (or at least starts to plateau in the case of HBPs) for mass scales $N = N_x$.

In Figure 12, we plot $N\upsilon_0\phi^2/l_p^3$ vs $N$ for HBPs for both $N_x < N_e$ (dashed line) and $N_x > N_e$ (solid line). We also show the critical number of binary contacts needed to form an entanglement $n'_c$ within the double reptation model (the intersection of $n'_c$ with the increasing portion of the $N\upsilon_0\phi^2/l_p^3$ curve defines

the entanglement degree of polymerization $N_e$). We see that for $N_x < N_e$, the maximum number of binary contacts always falls below the critical number required for entanglements. The analogous plot for percolation clusters is qualitatively the same except that $N\upsilon_0\phi^2/l_p^3 \sim N^{-1}$ for $N > N_x$ as we have already noted. Thus, the double reptation model also predicts that for $N_x < N_e$, both HBPs and percolation clusters are unentangled regardless of molecular weight.

**5.5. Other Issues.** Note that for the $N_x > N_e$ plot in Figure 10, the slope of the plot is negative for $N > N_x$ and the line eventually falls below $n_c$. However one should not conclude from this that HBP chains at the very high molar mass end of the distribution are unentangled. Recall that the purpose of Figure 10 (and Figure 12) was to see when the number of dynamically relevant contacts first exceeds $n_c$ in order to determine the entanglement molecular weight. For this reason, we assumed Rouse dynamics for the polymer chains. This results in mass scales and time scales being interchangeable which is crucial for the construction of the plot. The Rouse assumption is self-consistent below the entanglement molecular weight but breaksdown above the entanglement molecular weight. Everything on the plot to the right of the first point the line crosses $n_c$ is therefore unphysical. Instead, the relevant dynamics in this regime is the tube model (section 3.3.2) where time scales are associated with individual segments (rather than mass scales) and depend on the topological depth of the segment concerned within the tube. The same comments apply to the corresponding plots to Figures 10 and 12 for percolation clusters, where the slopes of the plots are also negative for $N > N_x$.

In summary, we have constructed a scaling argument that explains the entanglement transition for randomly branched polymers in both the HBP and percolation class. Note that in constructing our scaling model, it was important that we neglected the contribution from small side branches of large molecules. If we did not do so we would have to consider the volume fraction of all molecules larger than $N$ when calculating the dynamically relevant fraction of material contributing to entanglements. For HBPs, the dynamically relevant fraction now becomes $\phi = \int_N^\infty n(N')N'\,dN' \sim 1$ (for $N > N_x$). As a result, for $N > N_x$, the number of dynamically relevant binary contacts within the volume spanned by the mass scale $N$ now scales as $R(N)^3\phi^2/l_p^3 \sim N^{3/4}$ while the number of dynamically relevant binary contacts between a given chain with original mass $N$ and other chains now scales as $N\upsilon_0\phi^2/l_p^3 \sim N$. In both cases, the number of relevant binary contacts is now a monotonically increasing function of $N$ and no longer peaks at $N_x$. This would mean that both the Colby−Rubinstein and double reptation models predict that HBP chains can still be entangled even if $N_x < N_e$, which clearly disagrees with the experimental data. (For percolation clusters, the same argument would yield $\phi \sim N^{-1/2}$ for $N > N_x$ so that $R(N)^3\phi^2/l_p^3 \sim N^{-1/4}$ and $N\upsilon_0\phi^2/l_p^3 \sim N^0$. The conclusion that percolation clusters are unentangled for $N_x < N_e$ therefore remains unaffected.)

## 6. Conclusions

We have studied the melt rheology of randomly branched polymers in the hyperbranched polymer (HBP) class which are formed by the co-condensation of AB and $AB_2$ type monomers. Specifically motivated by the study of Colby and co-workers[4−6] on the percolation class, we have studied the effect of varying the branch length $N_x$ on the entanglement transition in the HBP class. To this end, two series of HBPs were prepared using $AB_2$ mole fractions of 10% (H10) and 1% (H1), respectively. This allowed us to vary the branch length $N_x$ from just below to just above $N_e$, the entanglement length for linear chains of the same chemistry.

For the H10 series ($N_x < N_e$), we were able to quantitatively model the low and intermediate frequency rheology data of the highest molecular weight samples using a dynamical scaling theory based on the Rouse model. However we found increasing deviations between theory and experiment with decreasing sample molecular weight. We attribute these discrepancies to a break down in dynamic scaling as we go to lower molecular weights. For the H1 series ($N_x > N_e$), there is a clear entanglement plateau for the higher molecular weight samples and we were able to quantitatively model the rheology around the entanglement plateau region using the tube model. However our tube model predicts a premature transition to terminal scaling, presumably because we have neglected the effect of branch length renormalization under dynamic dilution. Notwithstanding these discrepancies, the H10 and H1 rheology data demonstrate conclusively that the entanglement transition for randomly branched polymers in the HBP class is controlled by $N_x$ and the transition occurs around $N_x \approx N_e$. These conclusions are the same as for randomly branched polymers in the percolation class.

In the final section of the paper, we showed that these results can be explained using either the Colby−Rubinstein model or double reptation model for entanglements so long as we assume that whole molecules *and* side branches with Rouse times less than the Rouse time of an entanglement do not contribute to entanglement formation.

**Acknowledgment.** We are very grateful to Alexei Likhtman for fitting the rheology of the linear samples. DMAB and D.J.R. also gratefully acknowledge financial support from the EPSRC in the form of Advanced Research Fellowships.

## Appendix A. Details of the Tube Model

Because of the relatively low values of $b_U$ and $N_x$ for the H1 series, the branched ensemble consists primarily of linear or terminal species. We therefore use the star-linear blend theory of Milner and McLeish[42] as our starting point for constructing a tube model for our entangled HBPs. However we include the following important modifications.

First, in our theory, we account for the presence of "internal" spacers (with volume fraction $\phi_i$) which have seniority greater than 1. Second, Milner and McLeish develop their theory for the specific case where the dynamic dilution exponent $\alpha = 1$ while we generalize to arbitrary values of $\alpha$ (and later specialize to the case $\alpha = 4/3$). Third, for the entanglement spacing, we use the $G$ definition rather than the original $MM$ definition used by Milner and McLeish.[30] Within the $G$ definition, the entanglement spacing is defined to be

$$G_0 = \frac{4}{5}\frac{ckT}{N_e} \tag{11}$$

where $G_0$ is the experimentally measured plateau modulus and $c$ the number density of monomers. The above definition for the entanglement spacing was first proposed by Fetters et al.[2] (although it has also been attributed to an earlier paper by Graessley[63]) and it is used in a recent paper by Likhtman and McLeish.[28] It has the advantage of greatly reducing the number of "$^4/_5$" prefactors in the theory and also leads to much more intuitive relationships between the tube diameter $a$, the tube length $L$ and the entanglement spacing $N_e$ (i.e., $a = N_e^{1/2}b$ and $L = (N/N_e)a$).[28,30] Following Liktman and McLeish, we further

distinguish between the plateau modulus $G_0$ and the "entanglement modulus" $G_e$ which we define to be

$$G_e = \frac{ckT}{N_e} \tag{12}$$

so that $G_0 = {}^4/_5 G_e$. Finally we include Longitudinal Rouse modes[28] and fast Rouse motion inside the tube in our theory.

**A.1. Fast and Longitudinal Rouse Modes.** When an entangled polymer melt is deformed, it is assumed that the entanglement network (modeled by the tube) is deformed affinely.[64] This in turn deforms the polymer chains contained within the tube. The stress carried by chain deformations is initially relaxed via Rouse motion within a tube. The contribution of these modes to the complex modulus is given by[64]

$$G^*_{\text{Fast}} = G_e \frac{N_e}{N_x}\left[(\phi_i + \phi_l)\sum_{p=N_x/N_e}^{N_x} \frac{i\dfrac{\omega\tau_R}{2p^2}}{1 + i\dfrac{\omega\tau_R}{2p^2}} + \phi_t \sum_{p=N_x/N_e} \frac{i\dfrac{\omega\tau_R}{2(p - {}^1/_2)^2}}{1 + i\dfrac{\omega\tau_R}{2(p - {}^1/_2)^2}}\right] \tag{13}$$

where $\tau_R = (N_x/N_e)^2\tau_e$ and $\tau_e$ are the (rotational) Rouse relaxation times of a chain of length $N_x$ and $N_e$ respectively (the rotational Rouse relaxation time is twice the *stress* Rouse time). Note that the Rouse spectrum for linear chains (chains free at both ends) and internal chains (chains tethered at both ends) is different from that of terminal chains (chains tethered at one end only) and this is reflected in the above equation. Note also that we have only included the Rouse modes $p \geq N_x/N_e$ since lower Rouse modes are quenched by the tube.

For $2t < \tau_e$, although the entanglement network quenches free (i.e., 3D) Rouse motion, it still allows longitudinal (i.e., 1D) Rouse motion along the tube. These modes are able to relax ${}^1/_5$ of the stress carried by the entanglement network[28,64] and are the origin of the ${}^4/_5$ factor in eq 11. The contribution of these modes to the complex modulus is given by[28]

$$G^*_{\text{Long}}(\omega) = \frac{1}{5}G_e \frac{N_e}{N_x}\left[(\phi_i + \phi_l)\sum_{p=1}^{N_x/N_e} \frac{i\dfrac{\omega\tau_R}{p^2}}{1 + i\dfrac{\omega\tau_R}{p^2}} + \phi_t \sum_{p=1}^{N_x/N_e} \frac{i\dfrac{\omega\tau_R}{(p - {}^1/_2)^2}}{1 + i\dfrac{\omega\tau_R}{(p - {}^1/_2)^2}}\right] \tag{14}$$

Note that the longitudinal Rouse spectrum for linear chains and internal chains is again different from that of terminal chains[65] and this is reflected in the above equation. In what follows, we discuss mechanisms for relaxing the remainder of the stress ($G_0 = {}^4/_5 G_e$) carried by the entanglement network.

**A.2. Dynamic Dilution, $\tau < \tau_d$.** Before the reptation time of the linear chains $\tau_d$, terminal spacers (of length $N_x$) and the two "arms" of linear chains (each arm having the length $N_x/2$) can both relax via arm retraction (i.e., contour length fluctuations). The relaxation time $\tau_<(x)$ for an arm of length $N$ as a function of fractional distance $x$ retracted down the arm is given by solving the Ball−McLeish equation in the dynamically diluted regime

$$\frac{d(\log \tau)}{dx} = 2\nu x N/N_e(\Phi) = 2\nu n x \Phi(x)^\alpha \tag{15}$$

where in the $G$ definition, the constant $\nu = {}^3/_2$, $n = N/N_e$, and $\Phi$ is the unrelaxed volume fraction. The second equality comes from the assumption that the dynamically diluted entanglement spacing $N_e(\Phi)$ is given in terms of the undiluted entanglement spacing $N_e$ by

$$N_e(\Phi) = N_e \Phi^{-\alpha} \tag{16}$$

where $\alpha$ is the dynamic dilution exponent. Note that in the dynamic dilution regime, relaxation time scales can be expressed in terms of either $\tau$ or $x$ since the two are related via eq 13. Changing variables to $y = nx^2$, eq 13 becomes

$$\frac{d(\log \tau)}{dy} = \nu \Phi(y)^\alpha \tag{17}$$

which is independent of arm length $N$. Therefore, within Ball-McLeish theory, the fractional distance for terminal spacers $x$ is related to the fractional distance for the half-arm of a linear chain $x'$ via $n_x x^2 = y = n_x x'^2/2$, i.e., $x' = \sqrt{2x}$, where $n_x = N_x/N_e$.

Within the dynamic dilution regime, the volume fraction of unrelaxed material at the time scale corresponding to the fractional distance $x$ for terminal spacers (or $x'$ for linear chains) is given by

$$\Phi_<(x) = \phi_t(1 - x) + \phi_l(1 - x') + \phi_i = (1 - c_1 x) \tag{18}$$

where $c_1 = \phi_t + \sqrt{2\phi_l}$ and we have used $\phi_i + \phi_t + \phi_l = 1$ and $x' = \sqrt{2x}$ to obtain the second equality. Inserting eq 18 into eq 15 and solving, we find

$$\tau_<(x) = p_< \exp[U_<(x)] \tag{19}$$

where $U_<(x)$ is the effective potential against which terminal spacers undergo arm retraction and is given by

$$U_<(x) = 2\nu n_x \frac{1 - (1 - c_1 x)^{1+\alpha}(1 + c_1(1 + \alpha)x)}{c_1^2(1 + \alpha)(2 + \alpha)} \tag{20}$$

Within Ball−McLeish theory, the "attempt frequency" $p_<$ in eq 19 is a constant. However a more accurate expression for $\tau_<$ has been obtained by Milner and McLeish in an earlier paper.[66] This involves analyzing the longitudinal Rouse motion of a semiinfinite chain end at early times, solving the first passage problem for the free chain end at late times and constructing a crossover formula that interpolates between these two results. The final solution yields an effective attempt frequency in eq 19 which is a function of $x$ given by

$$p_<(x) = \left(\frac{1}{\tau_{\text{early}}(x)} + \frac{\exp(U_<(x))}{\tau_{\text{late}}(x)}\right)^{-1} \tag{21}$$

where

$$\tau_{\text{early}}(x) = \frac{9\pi^3}{16} n_x^4 \tau_e x^4 \tag{22}$$

and

$$\tau_{late}(x) = \frac{L^2}{D_{eff}}\left(\frac{2\pi}{U''_<(0)}\right)^{1/2}\frac{\exp(U_<(x))}{\left[U'_<(x)^2+\frac{2|U''_<(1)|}{\pi}\right]^{1/2}} \quad (23)$$

Within the G definition, $L^2/D_{eff} = 3/2n_x{}^3\pi^2\tau_e$ where $L = N_x/N_e$ is the tube length and $D_{eff} = 2D_R = 2k_BT/N_x\zeta$ is the effective diffusion coefficient of the chain end for a chain of length $N_x$ ($D_R$ is the Rouse diffusion coefficient of the chain and $\zeta$ is the monomeric friction coefficient). Note that the numerical prefactor in eq 22 is different from eq 13 in ref 66 and eq 7 in ref 42 because we are using the G definition (rather than MM definition) for the entanglement spacing.[30] Note also that eq 23 corrects an error of a factor of 2 and the omission of the absolute sign around $U''_<(1)$ in eq 21 of ref 66 and the spurious factor of $x^2$ in the denominator of eq 7 of ref 42 (see p 817 of ref 30).

The dynamic dilution regime ends at the reptation time of the linear chains $\tau_d$. The fractional distance a terminal arm has relaxed at the reptation time $x_d = x(\tau_d)$ is given by the solution of[42]

$$3n_x{}^3(1-\sqrt{x})^2\tau_e = \tau_<(x) \quad (24)$$

Note that the different numerical prefactor in the above equation compared to eq 9 of ref 42 is again due to our use of the G rather than MM definition for the entanglement spacing.

Within the dynamic dilution regime, it follows from eq 16 that the shear modulus associated with relaxation time scale $x$ is

$$G(x) = G_0\Phi^{1+\alpha} \quad (25)$$

where $G_0 = {}^4/_5G_e$ is the plateau modulus and $\Phi$ is the unrelaxed volume fraction given by eq 18.

**A.3. Constraint-Release Rouse Regime, $\tau_d < \tau < \tau_c$.** At relaxation times $\tau = \tau_d$, all linear chains essentially relax instantaneously and this results in a sudden drop of the unrelaxed volume fraction $\Phi$ (in fact $\Phi$ drops exponentially but we can approximate this as a step function on the time scale of contour length fluctuations). However one cannot assume that the tube diameter governing the relaxation of other chains increases as fast as $\Phi$ decreases because the unrelaxed chains explore their new larger tubes only gradually by a process known as constraint-release Rouse motion.[67] During constraint-release Rouse motion, dynamic dilution breaks down and the entanglement density is no longer controlled by $\Phi$ but a higher "supertube" fraction $\Phi_{ST}$. This is the volume fraction of entanglements that corresponding to the tube diameter that unrelaxed chains are actually able to explore in the time available (i.e., the "supertube" ).

Since chains explore their environment via Rouse-like motion in the constraint-release Rouse regime, the supertube diameter at relaxation times $\tau$ is given by $a(\tau)^4 \sim \tau$. On the other hand the supertube fraction is related to the supertube diameter via eq 16, but replacing $\Phi$ by $\Phi_{ST}$, i.e., $a(\Phi_{ST})^2 \sim N_e(\Phi_{ST}) \sim \Phi_{ST}{}^{-\alpha}$. Combining these two equations, we find that in the constraint-release Rouse regime, the supertube fraction at relaxation times $\tau$ is given by

$$\Phi_{ST}(\tau) = \Phi(\tau_d{}^-)\left(\frac{\tau_d}{\tau}\right)^{1/2\alpha} \quad (26)$$

where $\Phi(\tau_d{}^-) = \phi_i + \phi_t(1-x_d) + \phi_l(1-\sqrt{2x_d}) = 1 - c_1x_d$ is the volume fraction of unrelaxed material just before $\tau_d$. Equation 26 is the generalization of eq 12 in ref. 42 to general $\alpha$.

The constraint-release Rouse regime ends when the supertube fraction equals the unrelaxed volume fraction, i.e., when the supertube diameter catches up with the tube diameter corresponding to the fraction of unrelaxed material. Following Milner and McLeish, we assume that in the constraint-release Rouse regime, the effect of arm retraction on stress relaxation is negligible compared to constraint-release Rouse motion. This means that we can fix the unrelaxed volume fraction $\Phi$ to $\Phi(\tau_d^+) = \phi_i + \phi_t(1-x_d)$, the volume fraction of unrelaxed material just after $\tau_d$. The relaxation time corresponding to the end of the constraint-release Rouse regime is thus given by

$$\tau_c = \tau_d\left(\frac{\Phi(\tau_d{}^-)}{\Phi(\tau_d{}^+)}\right)^{2\alpha} \quad (27)$$

Since the entanglement density in the constraint-release Rouse regime is controlled by $\Phi_{ST}$, it follows that the shear modulus associated with the relaxation time $\tau$ is given by

$$G(\tau) = G_0\Phi\Phi_{ST}{}^{\alpha} = G_0(\phi_i + \phi_t(1-x_d))\Phi_{ST}(\tau)^{\alpha} \quad (28)$$

where $\Phi_{ST}(\tau)$ is given by eq 26.

**A.4. Recovery of Dynamic Dilution, $\tau > \tau_c$.** For $\tau > \tau_c$, dynamic dilution once again becomes valid and the entanglement volume fraction is once again equal to the volume fraction of unrelaxed material which is now given by

$$\Phi_>(x) = \phi_t(1-x) + \phi_i \quad (29)$$

Inserting eq 29 into the Ball−McLeish equation, eq 15, and solving, we find that the effective potential governing arm retraction in this regime is given by

$$U_>(x) = 2\nu n_x\frac{c_2{}^{2+\alpha} - (c_2-\phi_tx)^{1+\alpha}(c_2+\phi_t(1+\alpha)x)}{\phi_t{}^2(1+\alpha)(2+\alpha)} \quad (30)$$

where $c_2 = \phi_t + \phi_i$. The "attempt" frequency in this regime $p_>(x)$ can be obtained from eq 21, using $U_>(x)$ in place of $U_<(x)$. To ensure continuity of relaxation times across $\tau = \tau_c$, we write the relaxation time $\tau_>(x)$ in terms of $\tau_c$ as

$$\tau_>(x) = \tau_c\frac{p_>(x)}{p_>(x_d)}\exp[U_>(s) - U_>(s_d)] \quad (31)$$

In this regime, the shear modulus associated with the relaxation time scale $x$ is once again given by eq 25, but with the unrelaxed volume fraction now given by eq 29.

**A.5. Disentanglement Regime, $\tau > \tau_u$.** As stress relaxation proceeds, the volume fraction of unrelaxed material eventually becomes so low that the all the chains become disentangled. For samples which are highly branched and/or have long branch lengths, this disentanglement transition is negligible part of the total stress relaxation.[42,56] On the other hand, because of the relatively low values of $b_U$ and $N_x$ for the H1 series, the disentanglement transition is nonnegligible and needs to be considered explicitly.

However determining the exact point where disentanglement occurs is a nontrivial problem due to the possibility of branch-length renormalization (see section 4.5 and ref 56). For simplicity, we neglect branch-length renormalization and assume

that disentanglement occurs when the dynamically diluted entanglement length is equal to the undiluted branch length, i.e.,

$$N_e(\Phi_{ST}) = N_x \quad \text{or} \quad n_x {\Phi_{ST}}^{\alpha} = 1 \tag{32}$$

where $\Phi_{ST} = \Phi$ in the dynamic dilution regime. This condition defines a disentanglement time $\tau_u$. Thus, for all the dynamic regimes mentioned above, we first check that the condition $n_x {\Phi_{ST}}^{\alpha} > 1$ is satisfied throughout the regime, otherwise that relaxation regime is terminated at $\tau = \tau_u$ and replaced by terminal Rouse relaxation of the remaining unrelaxed material. For all the samples in the H1 series, $\tau_u$ occurs before the full relaxation of terminal spacers, i.e., within one of the three regimes mentioned in sections A.2 to A.4. For more highly branched and/or longer branch length samples, it is possible that $\tau_u$ occurs beyond the full relaxation of terminal spacers. In this case, one can readily extend our theory by adapting the theory of Blackwell et al.[21] (which considers well entangled Cayley trees) to highly entangled HBPs.

For $\tau > \tau_u$, the unrelaxed material can be considered to be an ensemble of unentangled "snipped" molecules in a Θ-solvent formed by the relaxed material. Noting that ${\tau_u}^{-1}$ plays the same role as $\epsilon_x$ in eq 2 and changing variables from $\epsilon$ to $\tau \equiv 1/\epsilon$, the complex shear modulus for $\tau > \tau_u$ is given by a simple extension of eq 2 as

$$G^*_{Slow}(\omega) = \Phi(\tau_u)\frac{d_R}{2}\frac{G_0\left(\frac{N_e}{N_x}\right)}{\Gamma(2-\tau, a)}\int_{\tau u}^{\infty}\left(\frac{\tau_u}{\tau}\right)^{(d_R/2)+1} \times \Gamma\left[2-\tau, a\left(\frac{\tau}{\tau_u}\right)^{d_R/2}\right]\frac{i\omega\tau}{1+i\omega\tau}\frac{d\tau}{\tau_u} \tag{33}$$

Here $G_0 = {}^4/_5 G_e$ is the plateau modulus, $d_R/2 = d_f/(d_f + 2) = 2/3$ (assuming $d_f = 4$) and $a = N_x/N_{char}(\Phi_u)$, where $N_{char}(\Phi_u) = N_{char}\Phi(\tau_u)$ is the largest characteristic degree of polymerization of the dynamically diluted ensemble.

**A.6. Shear Relaxation Modulus.** The contribution of the relaxation modes in sections A.2−A.4 to the complex modulus can be calculated from

$$G^*(\omega) = -\int_0^{\tau_u} d\tau \frac{dG(\Phi(\tau))}{d\tau}\frac{i\omega\tau}{1+i\omega\tau} = -\int_0^{x_u} dx \frac{dG(\Phi(x))}{dx}\frac{i\omega\tau(x)}{1+i\omega\tau(x)} \tag{34}$$

where the second expression is only applicable to the dynamic dilution regime where relaxation times can also be expressed in terms of $x$. Here $G(\tau)$ ($G(x)$) is the shear modulus associated with the relaxation time scale $\tau$ ($x$) and is given by eq 25 in the dynamic dilution regime and eq 28 in the constraint-release Rouse regime.

Inserting the relevant expressions for the shear modulus into eq 34, and combining with the high and low-frequency relaxation modes described in sections A.1 and A.5, respectively, the total complex modulus of the system is given by

$$G^*(\omega) = \frac{4}{5}G_e\left\{(\alpha+1)(\sqrt{2}\phi_l + \phi_t)\int_0^{x_d} dx \Phi_<(x)^{\alpha}\frac{i\omega\tau_<(x)}{1+i\omega\tau_<(x)} + \alpha(\phi_i + \phi_t(1-x_d))\int_{\tau_d}^{\tau_c} d\tau \frac{{\Phi_{ST}}^{\alpha}}{2\tau}\frac{i\omega\tau}{1+i\omega\tau} + (\alpha+1)\phi_t\int_{x_d}^{x_u} dx \Phi_>(x)^{\alpha}\frac{i\omega\tau_>(x)}{1+i\omega\tau_>(x)} + [\phi_i + \phi_t(1-x_d) + \phi_l(1-\sqrt{2}x_d)]^{\alpha}[\phi_l(1-\sqrt{2}x_d)]\frac{i\omega\tau_d}{1+i\omega\tau_d}\right\} + G^*_{Fast}(\omega) + G^*_{Long}(\omega) + G^*_{Slow}(\omega) \tag{35}$$

The first term in the above equation is the contribution from the arm retraction of terminal spacers and contour length fluctuations of linear chains before $\tau_d$ with $\Phi_<(x)$, $\tau_<(x)$ given by eqs 18 and 19, respectively. The second term is the contribution from constraint-release Rouse dynamics with $\Phi_{ST}$ given by eq 26. The third term is the contribution from arm retraction of terminal spacers after $\tau_c$ with $\Phi_>(x)$, $\tau_>(x)$ given by eqs 29 and 31, respectively. The fourth term is the contribution from the sudden drop in modulus from $G_0\Phi(\tau_d^-)\Phi^{\alpha}_{ST}(\tau_d)$ to $G_0\Phi(\tau_d^+)\Phi^{\alpha}_{ST}(\tau_d)$ at $\tau_d$ due to the reptation of linear chains. Finally $G^*_{Fast}(\omega)$, $G^*_{Long}(\omega)$, $G^*_{Slow}(\omega)$ are the contributions from fast, longitudinal and slow Rouse motion given by eqs 13, 14, and 33 respectively. Note that for definiteness we have assumed $\tau_u > \tau_c$ in eq 33. For $\tau_u < \tau_c$, the above expression is readily modified as explained in the previous section. Rather remarkably, eq 35 contains only three fitting parameters, namely $G_e$, $N_e$, and $\tau_e$, which are the entanglement modulus, spacing and Rouse time, respectively.

**Supporting Information Available:** Text giving the details of the reaction-kinetics model and txt files giving data files for the rheology results for the H1 and H10 series. This material is available free of charge via the Internet at http://pubs.acs.org.

## References and Notes


(1) Berry, G. C.; Fox, T. G. *Adv. Polym. Sci.* **1968**, *5*, 261.
(2) Fetters, L. J.; Lohse, D. J.; Richter, D.; Witten, T. A.; Zirkel, A. *Macromolecules* **1994**, *27*, 4639−4647.
(3) Ferry, J. D. *Viscoelastic Properties of Polymers*, 3rd ed.; John Wiley & Sons: New York, 1980.
(4) Colby, R. H.; Gillmor, J. R.; Rubinstein, M. *Phys. Rev. E* **1993**, *48*, 3712−3716.
(5) Lusignan, C. P.; Mourey, T. H.; Wilson, J. C.; Colby, R. H. *Phys. Rev. E* **1995**, *52*, 6271−6280.
(6) Lusignan, C. P.; Mourey, T. H.; Wilson, J. C.; Colby, R. H. *Phys. Rev. E* **1999**, *60*, 5657−5669.
(7) Flory, P. J. *J. Am. Chem. Soc.* **1952**, *74*, 2718−2723.
(8) Flory, P. J. *Principles of Polymer Chemistry;* Cornell University Press: Ithaca, NY, 1953.
(9) Hong, Y.; Cooper-White, J. J.; Mackay, M. E.; Hawker, C. J.; Malmstrom, E.; Rehnberg, N. *J. Rheol.* **1999**, *43*, 781−793.
(10) Hong, Y.; Coombs, S. J.; Cooper-White, J. J.; Mackay, M. E.; Hawker, C. J.; Malmstrom, E.; Rehnberg, N. *Polymer* **2000**, *41*, 7705−7713.
(11) Read, D. J.; McLeish, T. C. B. *Macromolecules* **2001**, *34*, 1928−1945.
(12) Benedikt, G. M., Goodall, B. L., Eds.; *Metallocene-Catalysed Polymers (Materials, Properties, Processing and Markets*); Plastics Design Library, William Andrew Inc.: New York, 1998.
(13) Lubensky, T. C.; Isaacson, J.; Obukhov, S. P. *J. Phys. (Paris)* **1981**, *42*, 1591−1601.
(14) Buzza, D. M. A. *Eur. Phys. J. E* **2004**, *13*, 79−86.
(15) de Gennes, P. G. *J. Phys. (Paris)* **1977**, *38*, L355−358.
(16) de Gennes, P. G. *Scaling Concepts in Polymer Physics;* Cornell University Press: Ithaca, NY, 1979.
(17) Suneel; Buzza, D. M. A.; Groves, D. J.; McLeish, T. C. B.; Parker, D.; Keeney, A. J.; Feast, W. J. *Macromolecules* **2002**, *35*, 9605−9612.

(18) Kasehagen, L. J.; Macosko, C. W.; Trowbridge, D.; Magnus, F. *J. Rheol.* **1996**, *40*, 689−709.
(19) McLeish, T. C. B.; O'Connor, K. P. *Polymer* **1993**, *34*, 2998−3003.
(20) Lee, A. T.; McHugh, A. J. *Macromolecules* **2001**, *34*, 9080−9086.
(21) Blackwell, R. J.; Harlen, O. G.; McLeish, T. C. B. *Macromolecules* **2001**, *34*, 2579−2596.
(22) Keeney, A. J. Thesis, University of Durham, 1998.
(23) Anderson, I. C. Thesis, University of Durham, 2000.
(24) For fractionation in THF as eluent, small secondary peaks were observed at small elution volumes for some HBP samples. These were initially believed to be due to aggregates which did not fit into any of the pores in the columns and hence elute together at early elution times before the exclusion limit of the columns. However we found that the addition of acetic acid suppressed the secondary peaks and we now believe that the small secondary peaks may instead be due to an ionic exclusion effect. This is where the sample accumulates partial negative charges due to the presence of polar carbonyl groups. The carbonyl groups induce charge in the eluent and therefore at the surface of the packing material. The polymer charges interact with partial charges on the surface of the packing material and result in "ionic exclusion", where the sample is repelled from the column media surface and is ejected from the column before the exclusion limit of the column. The addition of a little acetic acid suppresses the formation of charge and reduces ionic interaction, leading the sample to elute normally.
(25) Kunamaneni, S.; Buzza, D. M. A.; Parker, D.; Feast, W. J. *J. Mater. Chem.* **2003**, *13*, 2749−2755.
(26) Mourey, T. H.; Coll, H. In *Hyphenated Techniques in Polymer Characterization*; Advances in Chemistry 247; Provder, T., Ed.; American Chemical Society: Washington, DC, 1995.
(27) de Luca, E. Thesis, University of Durham, 2002.
(28) Likhtman, A. E.; McLeish, T. C. B. *Macromolecules* **2002**, *35*, 6332−6343.
(29) Tsenoglou, C. *Macromolecules* **1991**, *24*, 1762−1767.
(30) Larson, R. G.; Sridhar, T.; Leal, L. G.; McKinley, G. H.; Likhtman, A. E.; McLeish, T. C. B. *J. Rheol.* **2003**, *47*, 809−818.
(31) Feast, W. J.; Keeney, A. J.; Kenwright, A. M.; Parker, D. *Chem. Commun.* **1997**, *18*, 1749−1750.
(32) Parker, D.; Feast, W. J. *Macromolecules* **2001**, *34*, 2048−2059.
(33) Holter, D.; Frey, H. *Acta Polym.* **1997**, *48*, 298−309.
(34) Ball, R. C.; McLeish, T. C. B. *Macromolecules* **1989**, *22*, 1911−1913.
(35) McLeish, T. C. B.; et al. *Macromolecules* **1999**, *32*, 6734−6758.
(36) Das, C.; Inkson, N. J.; Read, D. J.; Kelmanson, M. A.; McLeish, T. C. B. *J. Rheol.* **2006**, *50*, 207−235.
(37) Rubinstein, M.; Colby, R. H.; Gillmor, J. R. In *Space-Time Organisation in Macromolecular Fluids*; Springer Series in Chemical Physics 51; Tanaka, F., Doi, M., Ohta, T., Eds.; Springer-Verlag: Berlin, 1989.
(38) Cates, M. E. *J. Phys. (Paris)* **1985**, *46*, 1059−1077.
(39) Chambon, F.; Petrovic, Z. S.; MacKnight, W. J.; Winter, H. H. *Macromolecules* **1986**, *19*, 2146−2149.
(40) Durand, D.; Delsanti, M.; Adam, M.; Luck, J. M. *Europhys. Lett.* **1987**, *3*, 297.
(41) Rubinstein, M.; Zurek, S.; Mcleish, T. C. B.; Ball, R. C. *J. Phys. (Paris)* **1990**, *51*, 757−775.
(42) Milner, S. T.; McLeish, T. C. B.; Young, R. N.; Hakiki, A.; Johnson, J. M. *Macromolecules* **1998**, *31*, 9345−9353.
(43) Costeaux, S.; Wood-Adams, P. *Macromolecules* **2002**, *35*, 2514.
(44) Rubinstein, M.; Colby, R. H. *Polymer Physics*; Oxford University Press: Oxford, U.K., 2003.
(45) See eq 6.122 in ref 44.
(46) Kunamaneni, S. Thesis, University of Leeds, 2003.
(47) Kunamaneni, S.; Buzza, D. M. A.; de Luca, E.; Richards, R. W. *Macromolecules* **2004**, *37*, 9295−9297.
(48) Randrianantoandro, H.; Nicolai, T.; Durand, D.; Prochazka, F. *Macromolecules* **1997**, *30*, 5893−5896.
(49) Nicolai, T.; Randrianantoandro, H.; Prochazka, F.; Durand, D. *Macromolecules* **1997**, *30*, 5897−5904.
(50) Pakula, T.; Vlassopoulos, D.; Fytas, G.; Roovers, J. *Macromolecules* **1998**, *31*, 8931−8940.
(51) Kapnistos, M.; Semenov, A. N.; Vlassopoulos, D.; Roovers, J. *J. Chem. Phys.* **1999**, *111*, 1753−1759.
(52) Vlassopoulos, D.; Fytas, G.; Roovers, J.; Pakula, T.; Fleischer, G. *Faraday Discuss.* **1999**, *112*, 225−235.
(53) Dorgan, J. R.; Knauss, D. M.; Al-Muallem, H. A.; Huang, T.; Vlassopoulos, D. *Macromolecules* **2003**, *36*, 380−388.
(54) See pp 191−193 in ref 3.
(55) Colby, R. H.; Rubinstein, M. *Macromolecules* **1990**, *23*, 2753−2757.
(56) Larson, R. G. *Macromolecules* **2001**, *34*, 4556−4571.
(57) Rubinstein, M. In *Theoretical Challenges in the Dynamics of Complex Fluids*; NATO ASI Series 339; McLeish, T. C. B., Ed.; Kluwer Academic Publishers: London, 1997.
(58) Milner, S. T. *Macromolecules* **2005**, *38*, 4929−4939.
(59) Brochard, F.; deGennes, P. G. *Macromolecules* **1977**, *10*, 1157−1161.
(60) desCloizeaux, J. *Europhysics Lett.* **1988**, *5*, 437−442.
(61) desCloizeaux, J. *Macromolecules* **1990**, *23*, 3992−4006.
(62) Adam, M.; Delsanti, M. *J. Phys. (Paris)* **1984**, *45*, 1513−1521.
(63) Graessley, W. W. *J. Polym. Sci., Part B: Polym. Phys.* **1980**, *18*, 27−34.
(64) Doi, M.; Edwards, S. F. *The Theory of Polymer Dynamics*; Clarendon Press: Oxford, U.K., 1986.
(65) Miros, A.; Vlassopoulos, D. *J. Rheol.* **2003**, *47*, 163−176.
(66) Milner, S. T.; McLeish, T. C. B. *Macromolecules* **1997**, *30*, 2159−2166.
(67) Viovy, J. L.; Rubinstein, M.; Colby, R. *Macromolecules* **1991**, *24*, 3587−3596.

MA0603276